2008-08-07

Magmatic Sulfur and Chlorine Abundances at Stromboli, Italy and their Role in the Formation of Vesicle-hosted Metal Alloys

Nichelle Lynn Baxter
Brigham Young University - Provo

MAGMATIC S AND CL ABUNDANCES AT STROMBOLI, ITALY AND THEIR ROLE IN THE FORMATION OF VESICLE-HOSTED METAL ALLOYS

by

Nichelle Baxter

A thesis submitted to the faculty of

Brigham Young University

in partial fulfillment of the requirements for the degree of

Master of Science

Department of Geological Sciences

Brigham Young University

December 2008

BRIGHAM YOUNG UNIVERSITY

GRADUATE COMMITTEE APPROVAL

of a thesis submitted by

Nichelle Baxter

This thesis has been read by each member of the following graduate committee and by majority vote has been found to be satisfactory.

Date	Jeffrey D. Keith, Chair
Date	Eric H. Christiansen
Date	Michael J. Dorais

BRIGHAM YOUNG UNIVERSITY

As chair of the candidate's graduate committee, I have read the thesis of Nichelle Baxter in its final form and have found that (1) its format, citations, and bibliographical style are consistent and acceptable and fulfill university and department style requirements; (2) its illustrative materials including figures, tables, and charts are in place; and (3) the final manuscript is satisfactory to the graduate committee and is ready for submission to the university library.

Date	Jeffrey D. Keith Chair, Graduate Committee

Accepted for the Department

Date	Scott M. Ritter Department chair

Accepted for the College

Date	Thomas W. Sederberg Associate Dean, College of Physical and Mathematical Science

ABSTRACT

MAGMATIC S AND CL ABUNDANCES AT STROMBOLI, ITALY AND THEIR ROLE IN THE FORMATION OF VESICLE-HOSTED METAL ALLOYS

Nichelle Baxter

Department of Geological Sciences

Master of Science

Strand et al. (2002) discovered small metal alloy grains rich in Cu, Co, and Sn (maximum size 150 μm) in vesicles of lava from Kilauea Volcano. These alloys are also found in basaltic rocks of several Italian volcanoes. To better understand the origin of these metal-rich grains, bombs from Stromboli Volcano were examined. Two bomb types were collected from Stromboli: pumiceous bombs and scoriaceous bombs. Bulk rock trace element geochemistry indicates that there are no significant differences in Cu, Co, or Sn (the three major components of the metal alloys) between the pumiceous and scoriaceous bombs. Comparison of olivine melt inclusion and matrix glass concentrations from these rocks shows that the pumiceous bombs are more primitive (melt inclusions: MgO 2.7-5.8 wt. %; matrix glass: MgO 5.1-6.50 wt. %) and are more S-rich (melt inclusions: maximum 0.13 wt. %; matrix glass: maximum 0.06 wt. %) than the

scoriaceous bombs. The melt inclusions and matrix glass in the scoriaceous bombs are more evolved (melt inclusions: MgO 3.0-4.3 wt. %; matrix glass: MgO 2.7-3.7 wt. %) and are S-poor (melt inclusions: maximum 0.06 wt. %; matrix glass: b.d.l.). However, Cl concentrations in melt inclusions and matrix glass are more similar for both bomb types. Metal alloys were counted in thin section for each sample. The crystallized interiors of the bombs contain more metal grains than the glassy exteriors. Pumiceous bombs (from more primitive, S-rich magma) contain more metal grains of a larger size than the scoriaceous bombs (from more fractionated, S-poor magma). This indicates that S (and Cl) are probable transport ligands for the metals in the alloys. As S (and Cl) move through the glass of an erupted cooling bomb, they complex with volatile chalcophile metals (Cu, Co, and Sn). These vapor-phase metal sulfides and chlorides move to inflating vesicles. Here the sulfide and chloride complexes become reduced and metal alloys condense, as S and Cl escape as gas. Non-degassed primitive magma may provide more S (but not necessarily more metals) to create the higher abundance of alloys hosted by the vesicles of the pumiceous bombs.

ACKNOWLEDGEMENTS

This thesis has only come to completion because of the generous support and contributions of many people. First of all, I would like to thank my thesis advisor Dr. Jeffrey Keith. I appreciate the opportunities Dr. Keith has given me to travel to so many places to see geology in action. Thank you so much for finding time in your very busy schedule to guide me along this path. I would also like to express my appreciation to Dr. Mike Dorais and Dr. Eric Christiansen for asking the hard questions and helping me to answer them. Many thanks to Megan Pickard for helping me to collect samples in Italy and Hawaii, and also for just putting up with me these past two years. Thank you to the rest of the BYU Geology department faculty and staff for all the help you have given me as well. Finally, I would like to thank my family for supporting me throughout this endeavor. I would never have finished this without their support.

List of Figures

List of Tables

Table of Contents

1. Introduction

Both magmatic aqueous and vapor phases rich in volatiles like sulfur and chlorine are able to complex with metals such as Cu, Co, Sn, Au, and Ag and strip them from magmas, moving them to other locations. Consequently, at an open conduit volcano, some of these metals and volatile-rich phases can "degass" from the magma.

One way that metal-rich sulfides and chlorides reach the surface is through the plumes of actively degassing volcanoes. Allard et al. (2000) documented sub-micron size sulfate and halide minerals as well as sulfate incrustations rich in Au, Cu, and Ag at the volcano Stromboli off the coast of Italy. They estimated that over the last 2 Ka years, Stromboli could have released enough Cu, Cr, Zn, and Au to be comparable to the amounts found in magma-derived high-sulfidation ore deposits.

Metal-bearing phases rich in sulfur and chlorine can also reach the surface through fumaroles. Sulfides rich in Cu, Cd, Fe, Pb, Mo, or Zn as well as Cu-. Pb-, and Zn-chlorides have been documented at a variety of fumaroles. Rarely, native Au has been documented as well (Williams-Jones and Heinrich, 2005).

Sulfur and chlorine can also be trapped in the vesicles of erupted material. Most recently, researchers documented a variety of metal-rich sulfide and chloride grains in the vesicles of samples from Mexico's Volcan Popocatepetl (Larocque et al., 2008). These sulfides and chlorides commonly contain precious and base metals like Ag, Au, and Cu. The researchers believe that these compounds were transported and deposited in the vesicles by a vapor phase.

Strand et al. (2002) discovered a new type of metallic grain consisting of Cu-Sn-Co alloys in vesicles of basaltic lavas from Kilauea and Pu'u 'O'o. Similar alloy grains have been found in mafic eruptive rocks from Vesuvius, Etna, Stromboli, Vulcano, and

Mauna Loa (Hunter, 2007). Hunter (2007) found that the relative amounts of Cu, Sn, and Co in the metal alloy grains vary from volcano to volcano. Kilauea rocks only host alloys that are rich in Cu (Cu>Sn>Co) whereas Vesuvius and Etna primarily host Co rich alloys (Co>Cu>Sn>Ag). Stromboli, however, hosts a significant amount of Cu-rich and Co-rich alloys. Some Stromboli rocks even host alloys rich in Ag. Hunter (2007) found that the surfaces of the alloys often have slightly higher concentrations of sulfur and chlorine. In some cases, the surfaces are coated with sulfides apparently deposited by vapor. This suggests that sulfur and chlorine are important components in the transport of the metals in the alloys from the cooling glass to the inflating vesicles. It is well documented that vapor-phase S and Cl can complex with and transport precious metals from magmas (Williams-Jones and Heinrich, 2005).

Stromboli not only hosts the most compositionally varied alloys, but it also hosts some of the largest alloys found at any of the volcanoes studied. As a consequence, Stromboli bombs were chosen for further investigation. To understand the role of S and Cl in the formation of these alloys, volatile concentrations in melt inclusions and matrix glass were studied from several Stromboli bombs. Bulk rock trace metal chemistry was also analyzed for these bombs to see if metal composition of the magma was important in the formation of the alloys as well.

2. Geological Setting

Stromboli is a stratovolcano that rises to 924 m above sea level and is located off the coast of Sicily (Fig. 1). It is the northeastern-most island of the Aeolian Islands. The Aeolian Arc formed as the Ionian microplate subducts under the Tyrhennian microplate (Gvirtzman et al., 1999).

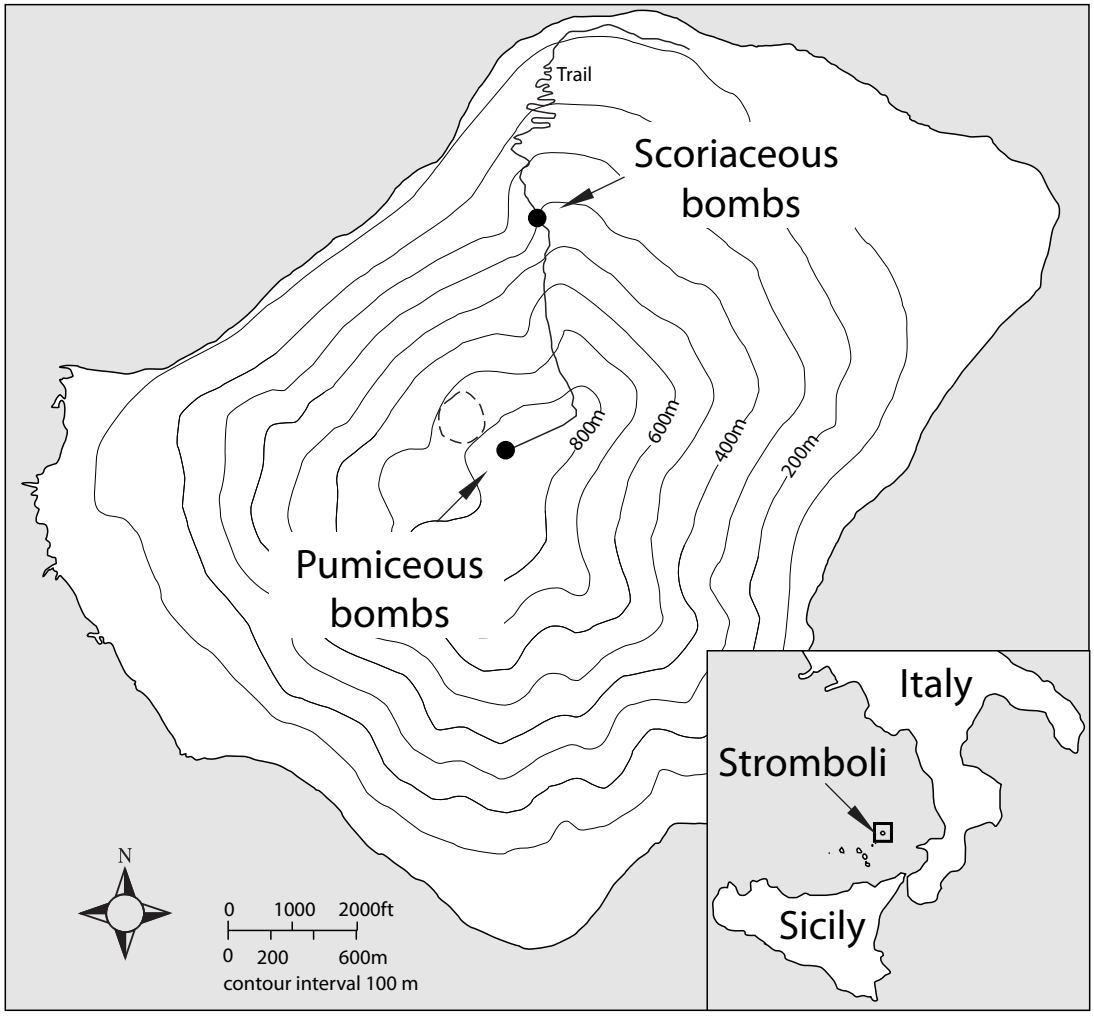

Figure 1. The volcano of Stromboli lies off the coast of mainland Italy. Sample locations are marked as filled circles along the north trail leading to the summit of the volcano. The active vent is outlined by a dashed line.

Stromboli started to form 110 Ka. The geochemistry of the volcano has changed over time, varying between high-K calc-alkaline (HKCA), calc-alkaline, potassic, and shoshonitic (classification according to SiO_2 vs K_2O diagram; Francalanci et al., 1993). These changes in composition were sometimes marked by violent sector collapse and oxidizing conditions in the magma chamber (Cortes et al., 2006; Francalanci et al., 1989). Recent activity started about 6 Ka and has been characterized by HKCA and shoshonitic eruptions (Laiolo et al., 2006; Cortes et al., 2005; Keller et al., 1993; Francalanci et al., 1989).

Stromboli has been erupting consistently in its present style for the last 1400-1800 years (Rosi et al., 2000). Its eruptive style is generally strombolian but has been interspersed with effusive activity every 10 to 20 years and has rare explosive "paroxysms" (Laiolo et al., 2006). The transition between these different types of eruptions is controlled by the magma volume and the level of the magma in the conduit (Landi et al., 2006), which are both related to the gas flux (Ripepe et al., 2005). Degassing is continuous and releases 6,000 to 12,000 metric tons per day of H_2O, CO_2, SO_2, HCl, and HF (Allard et al., 1994). Today's activity (consisting of strombolian eruptions with rare lava flows or paroxysms) has been characterized by high-K-calc-alkaline and shoshonitic volcanism (Laiolo et al., 2006).

Crystal-rich, degassed (low levels of volatiles such as S and Cl) basaltic scoria is emitted in the normal strombolian activity and in the effusive episodes. In contrast, the explosive paroxysms erupt high-K 'golden' pumice (crystal-poor and volatile-rich) as well as crystal-rich, degassed scoria (Metrich et al., 2001; Francalanci et al., 2004). The golden pumice and scoria differ in both bulk-rock and mineral composition. Both rock

types vary from high-K to shoshonitic basalts. Bulk rock compositions indicate that the golden pumice is slightly less evolved than the scoria. This is evident in slightly lower SiO_2 and K_2O concentrations and more primitive olivine, clinopyroxene, and plagioclase compositions in the golden pumice (Francalanci et al., 2004). The scoria contains 45-60 vol% phenocrysts and microphenocrysts of plagioclase>clinopyroxene>olivine (Francalanci et al., 2004). It is more evolved and relatively degassed (Metrich et al., 2001). The golden pumice contains <10 vol% phenocrysts of olivine, clinopyroxene, and plagioclase (Francalanci et al., 2004). Olivine-hosted melt inclusion data indicates that the golden pumice is more primitive (CaO-rich, FeO-poor) and volatile-rich than the scoria (Metrich et al., 2001; Bertagnini et al., 2003).

Metrich et al. (2001) proposed a model where the scoria is erupted in strombolian eruptions from an actively degassing magma in the cone of the volcano (100 MPa). On the other hand, the golden pumice comes from volatile-rich magma that originates deeper in the volcano (~270 MPa; di Carlo et al., 2006) and rises quickly to the surface before it can substantially degass. It erupts explosively in rare paroxysms and forms the golden pumice. Francalanci et al. (2005) found evidence for mixing between the volatile-rich (golden pumice) and volatile-poor (scoria) magmas. They found large variations in Sr isotopes in plagioclase and clinopyroxene from both scoria and pumice samples. They interpreted these variations to mean that the volatile-rich and volatile-poor magmas were mixing in the shallow magma reservoir shortly before eruption.

3. Methods

3.1 Sampling

Bombs of golden pumice and scoria were collected from Stromboli. Pumiceous bombs were collected at the top of the volcano (Strom1 and Strom5). These bombs are

gold in color and are highly vesicular. They contain ~10-15 % phenocrysts of plagioclase, clinopyroxene, and olivine with the bulk of the rock composed of glass/crystallized matrix and vesicles (Fig. 2). The bombs have a cow-pie morphology and are the youngest deposit at the sample location.

Scoriaceous bombs were collected from the north trail at about 480 m a.s.l. (Strom07-1, Strom07-2, Strom07-5). These samples are dark grey to black and are more dense than the pumiceous bombs. The scoriaceous bombs are also more phenocryst-rich (~50% phenocrysts of plagioclase, clinopyroxene, and olivine) than the pumiceous bombs (Fig. 2). More detailed sample descriptions are found in Appendix 8.1.

Thin sections were prepared for each sample along the outer glassy rind of the bombs, to preserve fresh, uncrystallized matrix glass for analysis. Additional thin sections of the interior of the bombs were prepared for several samples as well. In order to preserve the metal alloys found in the vesicles of the samples, the thin sections were vacuum impregnated with epoxy before the thin sections were cut.

3.2 Metal alloy proportions

Equal areas of thin sections from the crystallized interiors and glassy rinds of the bombs were optically examined for grains of metal alloys at 20x magnification in reflected light. Only yellow-gold, highly reflective grains were included in the results.

3.3 Electron microprobe analysis of melt inclusions and matrix glass

Melt inclusions in olivine were analyzed both in thin section and from mineral separates (see Appendix 8.2 for technique). Melt inclusions in clinopyroxene were only analyzed in thin section. Suitable melt inclusions were selected by ensuring that the melt inclusions were larger than 10 microns and no secondary crystallization was visually

a. Scoriaceous bombs (from strombolian eruptions)

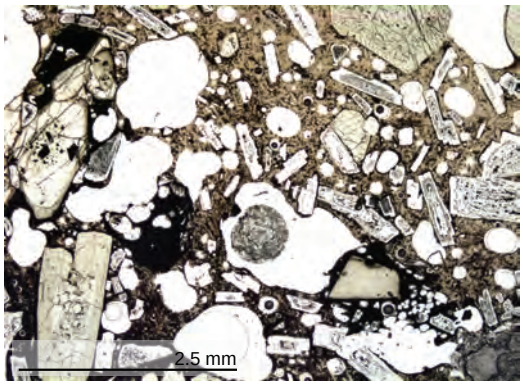

b. Pumiceous bombs (from rare paroxysms)

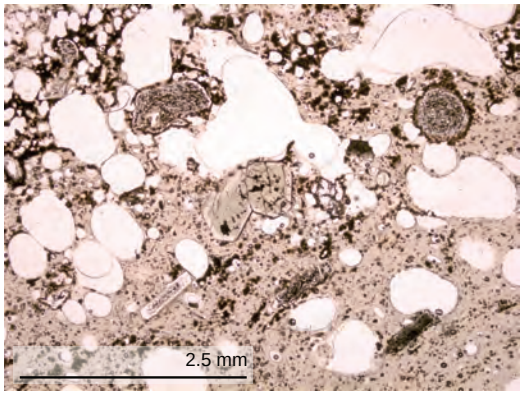

Figure 2. Representative images and photomicrographs of the two types of bombs studied. a. The scoriaceous bombs (most common material erupted today) are dark and dense with ~50% phenocrysts of plagioclase, clinopyroxene, and olivine. b. The pumiceous bombs (erupted in rare paroxysms) are a dark yellow-brown with ~10-15% phenocrysts of plagioclase, clinopyroxene, and olivine.

evident under the microscope. Because of the general scarcity of melt inclusions in the samples, some fractured inclusions were also analyzed.

Melt inclusions and matrix glass were analyzed using a Cameca SX50 electron microprobe with a beam current of 10 nA, a beam size of 10 microns, and a counting time of 20 s . A barite standard was used for sulfur and a scapolite standard was used for chlorine. Minerals were analyzed in thin section using a beam current of 20 nA, a minimum beam size, and a counting time of 20 s.

Melt inclusions in olivine were corrected for postentrapment crystallization after Luhr (2001) assuming that 20 at% of the Fe^t is Fe^{3+} at Stromboli (Bertagnini et al., 2003).

3.4 Element Dot Maps

Element concentration maps were created for S and several major elements using a Cameca SX50 electron microprobe. With a magnification of 100 µm, a stage scan was used with a beam current of 200 nA and a beam size of 10 microns. Pixel time was 50 ms with a definition of 256x256. With this setting, major elements SiO_2, FeO, and MgO as well as S were successfully imaged. S was also imaged at a smaller scale. With a magnification of 500 µm, a beam scan was used with a beam current of 200 nA and the beam size of 10. Pixel time was 50 s and definition was 256x256. At these settings, images for SiO_2, FeO, or MgO were not successfully created because of the loss of intensity due to the defocusing effect caused by the higher magnification. Sulfur variations were clearer, however.

3.5 Whole rock metal compositions

Samples were analyzed for a variety of trace elements including important base and precious metals at the Vancouver ALS Chemex lab. Au, Pt, and Pd were analyzed

using fire assay fusion and Plasma Emission Spectroscopy (ICP-AES). S was analyzed by a Leco furnace technique. The other trace elements were analyzed by processing the samples with 4-acid 'near total' digestion and then analyzing them using Inductively Coupled Plasma Mass Spectroscopy (ICP-MS) and ICP-AES.

4. Results

4.1 Whole rock chemistry

Only small differences in trace element chemistry were found between the pumiceous and scoriaceous bombs (Fig. 3; Appendix 8.3). When averaging the analyses for both bomb types, the pumiceous bombs contain slightly higher amounts of Au (0.004 ppm), Pd (0.0085 ppm), Cu (104.95 ppm), Re (0.005 ppm), Sr (762 ppm), and Tl (0.22 ppm) than the scoriaceous bombs (Au: 0.002 ppm; Pd: 0.005 ppm; Cu: 99.97 ppm; Re: 0.003 ppm; Sr: 744 ppm; Tl: 0.08 ppm). The scoriaceous bombs contained slightly higher concentrations of other elements including Pt (0.006 ppm), Ag (0.20 ppm), Li (9.7 ppm), Rb (53.9 ppm), and Th (15.1 ppm) than the pumiceous bombs (Pt: 0.005 ppm; Ag: 0.12 ppm; Li: 8.9 ppm; Rb: 33.9 ppm; Th: 10 ppm). Whole-rock S was slightly higher in the pumiceous bombs as well, with sample Strom1 containing the highest amount. However, average concentrations of the three main components (Cu, Co, and Sn) found in the metal alloy grains are similar in both the pumiceous (Cu: 105 ppm; Co: 32.4 ppm ; Sn: 1.7 ppm) and scoriaceous bombs (Cu: 100 ppm; Co: 32.1 ppm ; Sn: 1.7 ppm). When comparing each rock sample to the average of the scoriaceous bomb samples (Fig. 3), it is apparent that S appears to be the only element that is dramatically different between the pumiceous bombs and scoriaceous bombs. There are other small differences in Se, Rb, Pd, In, Pt, Au, and Tl, but the sample size of this study is too small to make any conclusions from the data.

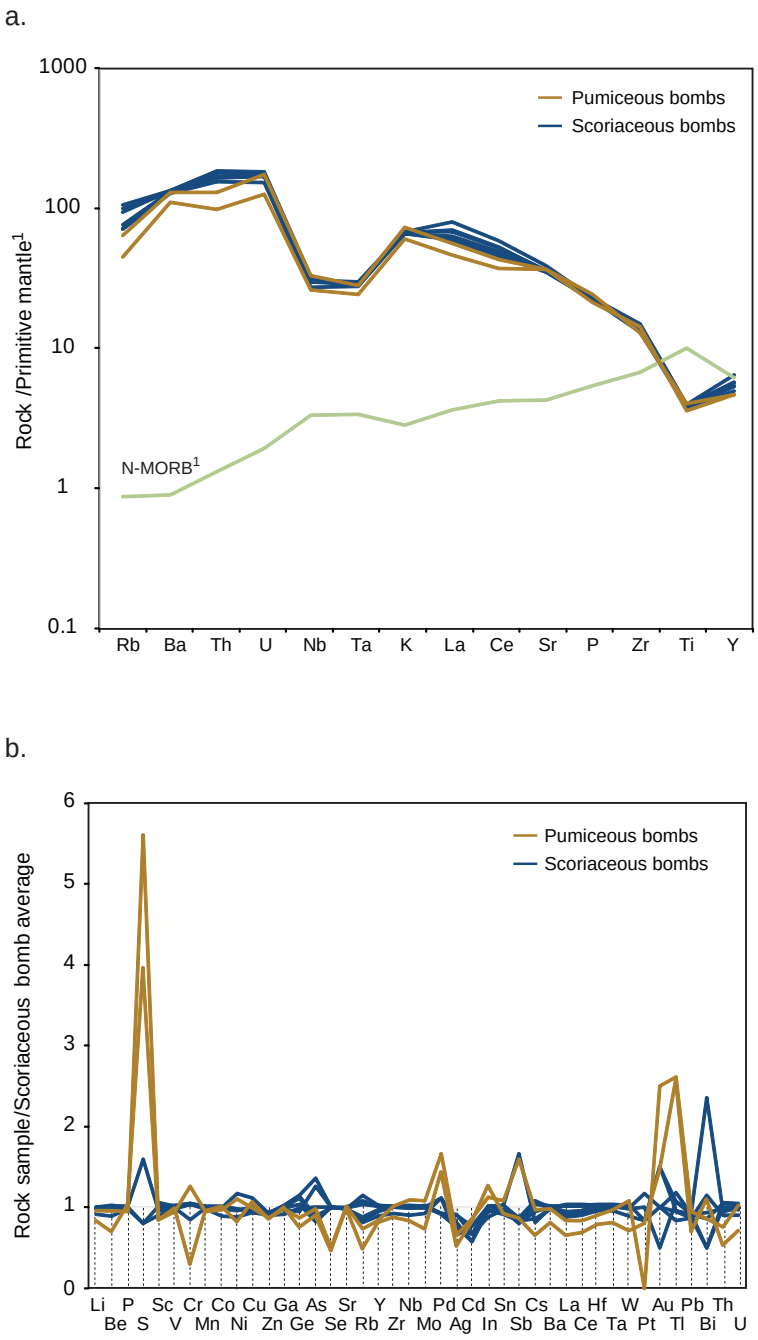

Figure 3. Trace element diagrams of pumiceous and scoriaceous bombs. a. Spider diagram of pumiceous and scoriaceous bombs. The pumiceous and scoriaceous bombs have very similar trace element distributions. b. Ratio of each rock sample to the average composition of the scoriaceous bombs. The only major difference between the two pumiceous and scoriaceous bombs is in S.
[1] from Sun and McDonough (1995)

4.2 Mineral Chemistry

The pumiceous bombs and scoriaceous bombs are noticeably different from one another in their mineralogy, both modally and chemically. The pumiceous bombs contain clinopyroxene, plagioclase, and olivine with total phenocryst content only at ~10-15%. The scoriaceous bombs contain clinopyroxene, plagioclase, and olivine with total phenocryst content at ~50% (more detailed sample descriptions in appendix 8.1). Based on mineralogical evidence, the pumiceous bombs and scoriaceous bombs are very similar to the golden pumice and scoria erupted at Stromboli today.

4.2.1 Olivine

The pumiceous bombs contain three types of olivine and are compared to olivine in the golden pumice and scoria in Figure 4 (Table 1; for full table of analyses see Appendix 8.4). The first type is comprised of euhedral olivine with a small range in composition (Fo_{71-72}). These homogenous olivine grains have little or no zoning. The second type of olivine is commonly resorbed and reversely zoned with abundant but small melt inclusions and embayments. The cores of these olivine grains range from Fo_{66-72} and the rims range from Fo_{80-88}. The third type of olivine is homogeneous with a small range in composition that is more MgO rich (Fo_{82-83}) than the first type of olivine. These more primitive olivines are rich in melt inclusions and embayments. One olivine with dramatic normal zoning was found in Strom1 (Core: Fo_{82} ; Rim: Fo_{69}). Overall, the olivine phenocrysts from the pumiceous bombs have a large compositional range (Fo_{67-88}), but there is also a noticeable gap in the olivine compositions between MgO wt. % 36.8 and 39.5 (Fo_{73} and Fo_{77}).

The olivine compositions from the pumiceous bombs are consistent with what has previously been documented in the golden pumice. Bertagnini et al. (2003), Francalanci

Table 1. Representative olivine compositions from pumiceous and scoriaceous bombs

Pumiceous bombs

	strom1olv3	strom1olv3	strom5-olv1	strom5-olv1	strom5olv1	strom5olv1
	core	rim	core	rim	core	rim
SiO_2	39.93	40.38	37.27	36.92	37.45	39.59
TiO_2	0.02	0.00	0.02	0.02	0.03	0.01
Al_2O_3	0.02	0.05	0.05	0.03	0.04	0.04
FeO	15.51	15.58	26.47	26.07	28.35	18.50
MnO	0.27	0.26	0.51	0.49	0.50	0.32
NiO	0.18	0.13	0.06	0.02	0.00	0.07
MgO	44.00	44.03	36.03	36.54	33.43	41.44
CaO	0.28	0.31	0.36	0.35	0.29	0.29
Total	100.19	100.74	100.75	100.42	100.09	100.26
Fo	83.56	83.57	70.77	71.39	67.66	80.01
Mg#	0.83	0.83	0.71	0.71	0.68	0.80

Scoriaceous bombs

	strom07-1 olv2	strom07-1 olv2	strom07-2 olv4	strom07-2 olv4	strom07-5 olv2	strom07-5 olv2
	core	rim	core	rim	core	rim
SiO_2	38.38	38.26	36.80	37.18	37.37	37.36
TiO_2	0.00	0.02	0.01	0.03	0.01	0.02
Al_2O_3	0.04	0.04	0.01	0.02	0.03	0.04
FeO	23.44	24.18	24.77	24.33	24.16	24.35
MnO	0.42	0.45	0.46	0.47	0.46	0.44
NiO	0.11	0.00	0.07	0.03	0.05	0.11
MgO	37.08	36.65	37.04	36.74	36.75	36.70
CaO	0.37	0.36	0.31	0.35	0.31	0.32
Total	99.83	99.96	99.46	99.14	99.13	99.33
Fo	73.87	72.99	72.66	72.90	73.01	72.85
Mg#	0.74	0.73	0.73	0.73	0.73	0.73

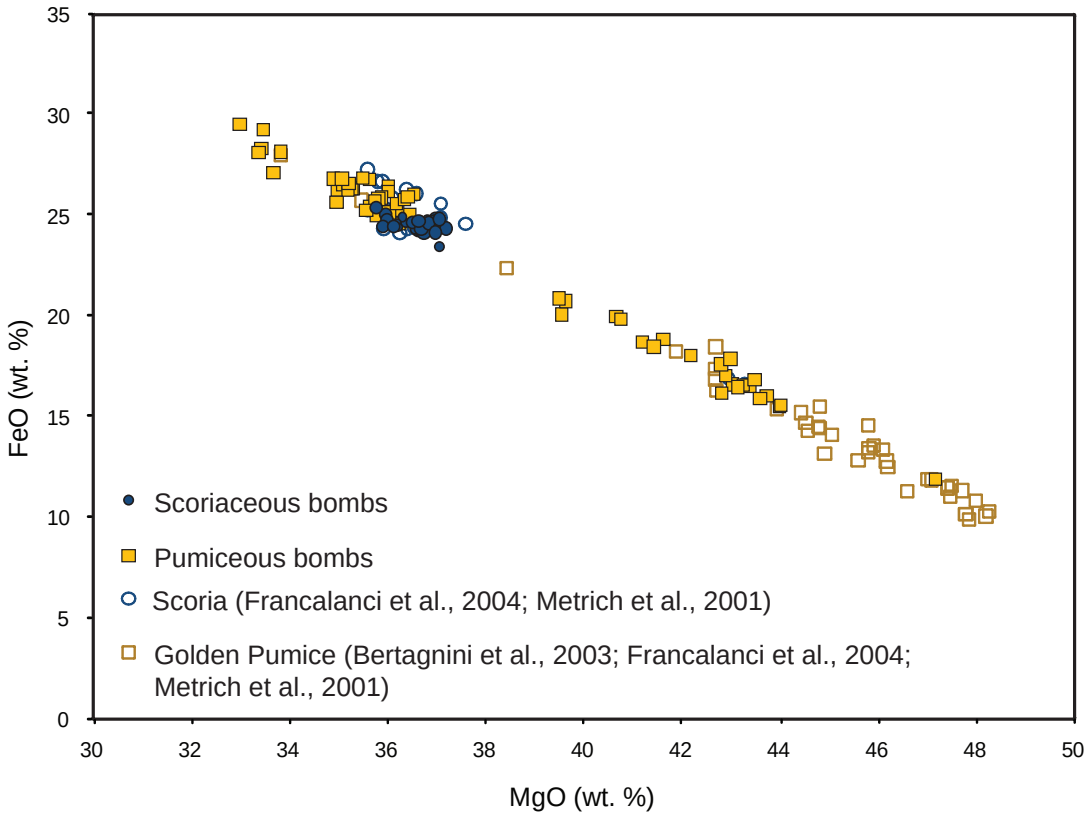

Figure 4. MgO versus FeO in olivine from scoriaceous and pumiceous bombs. The scoriaceous bombs contain Fe-rich olivine with less variation than the pumiceous bombs. The scoriaceous and pumiceous olivine are comparable to the scoria and golden pumice olivine respectively (Bertagnini et al., 2003; Francalanci et al., 2004; Metrich et al., 2001), although the pumiceous bombs do not contain the most primitive compositions the golden pumice contains.

et al. (2004), and Metrich et al. (2001) have recorded large variations in golden pumice olivine compositions (Fo_{66-86}) comparable to the variations found in the pumiceous bombs. They have found several different olivine populations, including more evolved, homogenous olivine (Fo_{64-74}; comparable to the first olivine group from the pumiceous bombs), a variety of reversely-zoned olivine (Core: Fo_{68-74}, Rim: Fo_{80-86}; comparable to the second olivine group from the pumiceous bombs), more primitive, homogeneous olivine (Fo_{87}, Fo_{83}; comparable to the third olivine group from the pumiceous bombs), as well as rare, very primitive, normally zoned olivine (Fo_{91-86}).

It is important to note that the pumiceous bombs did not have the most primitive olivines found in the golden pumice. The pumiceous bombs only contained olivine cores with a maximum composition of Fo_{83}, whereas the golden pumice studied by Bertagnini et al. (2003), Francalanci et al. (2004), and Metrich et al. (2001) contained olivine with a maximum composition of Fo_{91}. This could be because the rocks in this study are larger 'cow-pie' bombs sampled from a slightly more evolved magma, whereas the golden pumice studied in the past came from a slightly more primitive magma.

The three scoriaceous bombs contain homogeneous olivine that is generally euhedral (Fo_{72-74}; Table 1; Fig. 5), similar to those described by others. Francalanci et al. (2004) and Metrich et al. (2001) have shown that the scoria contains more evolved olivine with a much smaller range in composition (Fo_{64-75}) than the golden pumice. The difference between the olivines in the two magma types is easily seen in backscatter electron images (Fig. 5). The pumiceous bombs contain many olivines with obvious reverse or normal zoning, whereas there is no zoning found in the olivines from the scoriaceous bombs.

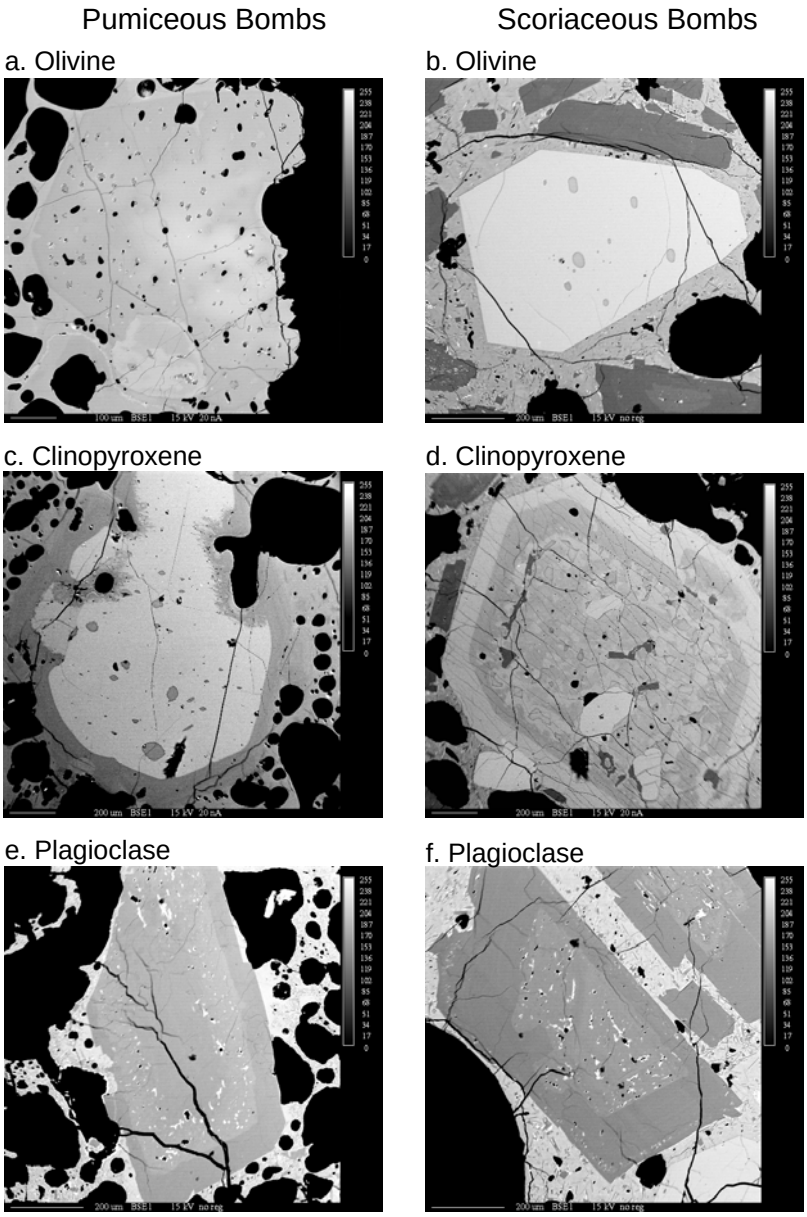

Figure 5. Backscatter electron images of major phenocrysts from both types of bombs. a. One of several types of olivine found in the golden pumice. This olivine is reversely zoned with a MgO-rich rim. b. All of the olivine in the scoriaceous bombs is fairly homogenous with little or no zoning and is more evolved than the pumiceous bombs, as seen in this image. c. Many of the clinopyroxene phenocrysts in the pumiceous bombs have a distinct, thin diopsidic rim, which is evident in this image. d. The clinopyroxene from the scoriaceous bombs have complex zoning and all of them have a thicker augitic rim in comparison to the pumiceous bombs. e. Plagioclase from the pumiceous bombs have complex zoning and high An content. f. Plagioclase from the scoriaceous bombs also have complex zoning but they are not as anorthitic as the plagioclase from the pumiceous bombs.

4.2.2 Clinopyroxene

The pumiceous bombs contain euhedral clinopyroxene grains that range in composition from $Wo_{39}Fs_{7}$ to $Wo_{47}Fs_{18}$ (Table 2; Fig. 6; see appendix 8.5 for full data set). The clinopyroxenes are commonly reversely zoned with a thin diopsidic rim (Wo_{47-42}) and a higher Mg# ranging from 85.8 to 87.3. Likewise, Francalanci et al. (2004) and Metrich et al. (2001) found that the rims in clinopyroxene from the golden pumice were commonly thin and diopsidic. These rims can easily be seen in back scatter electron images (Fig. 6). Francalanci et al. (2004) hypothesized that the augitic cores of the reversely zoned clinopyroxene were xenocrysts from the shallow degassed magma (scoria). When the more volatile-rich magma mixed with the degassed magma, diopsidic rims grew on the augitic clinopyroxene cores.

On the other hand, the scoriaceous bombs contain euhedral clinopyroxene grains that have a smaller range in composition ($Fs_{9}Wo_{41}$ to $Fs_{15}Wo_{45}$). The clinopyroxenes are complexly zoned and have cores that are sometimes partially resorbed. The rims of these clinopyroxenes are usually thicker than those in the pumiceous bombs and are always augitic (Wo_{45-43}; Fig. 5). This is consistent with the augitic, complexly zoned clinopyroxene found by others. Francalanci et al. (2004) and Metrich et al. (2001) found that the scoria contained pyroxene with resorbed cores and thick augitic rims. Patchy zoning was also common.

4.2.3 Plagioclase

The plagioclase in both types of bombs is commonly zoned with sieve textures. In the scoriaceous bombs, plagioclase varies from An_{86-66}, whereas in the pumiceous bombs, plagioclase has a larger variation of An_{89-61}(Table 3; Fig. 7; see appendix 8.6 for full data

Table 2. Representative analyses of clinopyroxene from pumiceous and scoriaceous bombs

Pumiceous bombs

	strom1 cpx5 core	strom1 cpx5 rim	strom1 cpx7 core	strom1 cpx7 rim	strom5 cpx4 core	strom5 cpx4 rim
SiO_2	51.36	51.26	49.53	51.40	51.64	50.93
TiO_2	0.72	0.50	0.87	0.55	0.62	0.59
Al_2O_3	2.87	4.30	4.72	4.68	3.00	5.03
FeO	8.89	4.41	8.93	4.69	8.34	4.64
MnO	0.24	0.10	0.20	0.11	0.28	0.10
MgO	14.70	16.21	13.34	15.85	14.73	15.65
CaO	20.36	22.35	21.09	22.22	20.86	22.66
Na_2O	0.36	0.21	0.35	0.26	0.36	0.17
Total	99.50	99.32	99.02	99.74	99.83	99.77
En	0.43	0.47	0.40	0.46	0.43	0.45
Fer	0.15	0.07	0.15	0.08	0.14	0.08
Wo	0.43	0.46	0.45	0.46	0.44	0.47
Mg#	0.75	0.87	0.73	0.86	0.76	0.86

Scoriaceous bombs

	strom07-1 cpx1 core	strom07-1 cpx1 rim	strom07-2 cpx3 core	strom07-2 cpx3 rim	strom07-2 cpx5 core	strom07-2 cpx5 rim
SiO_2	53.08	50.49	51.37	50.91	50.18	50.50
TiO_2	0.46	0.92	0.71	0.92	1.04	0.93
Al_2O_3	1.90	3.75	3.01	3.65	4.02	3.65
FeO	5.45	7.86	7.33	7.86	8.98	7.86
MnO	0.18	0.22	0.20	0.21	0.22	0.21
MgO	16.75	14.47	15.22	14.65	13.89	14.77
CaO	21.51	21.13	21.09	20.93	20.80	21.08
Na_2O	0.23	0.29	0.29	0.29	0.34	0.31
Total	99.55	99.12	99.21	99.42	99.46	99.32
En	0.47	0.42	0.44	0.43	0.41	0.43
Fer	0.09	0.13	0.12	0.13	0.15	0.13
Wo	0.44	0.45	0.44	0.44	0.44	0.44
Mg#	0.85	0.77	0.79	0.77	0.73	0.77

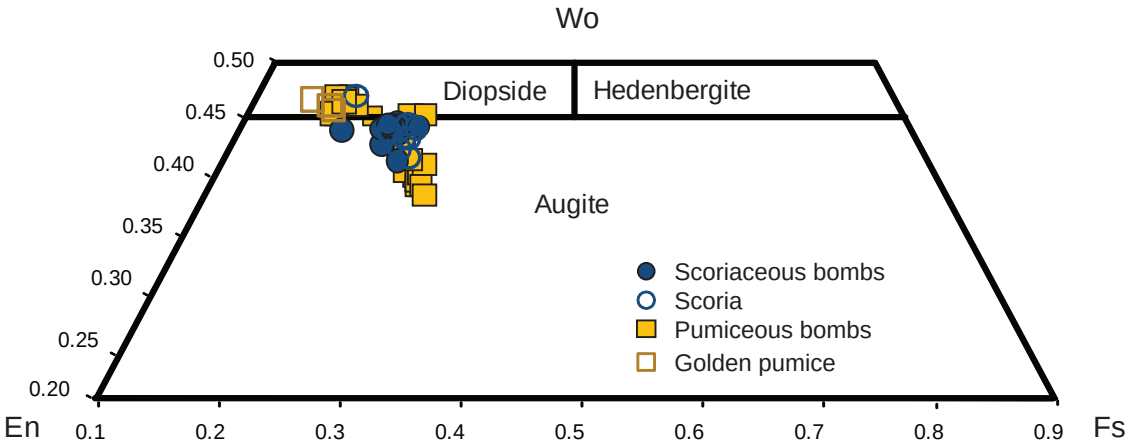

Figure 6. The scoriaceous bombs contain clinopyroxene with augitic cores and rims , whereas the pumiceous bombs have augitic cores and diopsidic rims . Diopsidic rims have been documented in the golden pumice, whereas the scoria has augitic rims (data taken from Francalanci et al., 2004).

Table 3. Representative plagioclase analyses for pumiceous and scoriaceous bombs

Pumiceous bombs

	strom1 plag3	strom1 plag3	strom1 plag4	strom1 plag4	strom1 plag5	strom1 plag5
	core	rim	core	rim	core	rim
SiO_2	47.07	46.21	46.07	45.99	45.74	46.00
Al_2O_3	34.04	33.45	34.73	34.52	34.49	34.23
Fe_2O_3	0.43	0.58	0.55	0.58	0.56	0.58
CaO	17.64	16.98	18.19	18.12	17.94	17.64
Na_2O	1.59	1.66	1.10	1.18	1.27	1.37
K_2O	0.16	0.18	0.08	0.08	0.10	0.15
Total	100.92	99.06	100.71	100.48	100.10	99.97
Ab	0.14	0.15	0.10	0.10	0.11	0.12
An	0.85	0.84	0.90	0.89	0.88	0.87
Or	0.01	0.01	0.00	0.00	0.01	0.01

Scoriaceous bombs

	strom07-1 plag1	strom07-1 plag1	strom07-1 plag2	strom07-1 plag2	strom07-1 plag4	strom07-1 plag4
	core	rim	core	rim	core	rim
SiO_2	52.13	47.02	47.29	48.79	47.74	51.10
Al_2O_3	29.99	33.41	32.99	31.10	32.37	30.59
Fe_2O_3	0.69	0.94	0.84	0.98	0.84	0.68
CaO	12.82	17.04	16.89	14.57	15.83	13.61
Na_2O	3.85	1.75	1.85	2.86	2.34	3.43
K_2O	0.74	0.23	0.22	0.49	0.34	0.59
Total	100.21	100.38	100.09	98.80	99.47	100.00
Ab	0.34	0.15	0.16	0.25	0.21	0.30
An	0.62	0.83	0.82	0.72	0.77	0.66
Or	0.04	0.01	0.01	0.03	0.02	0.03

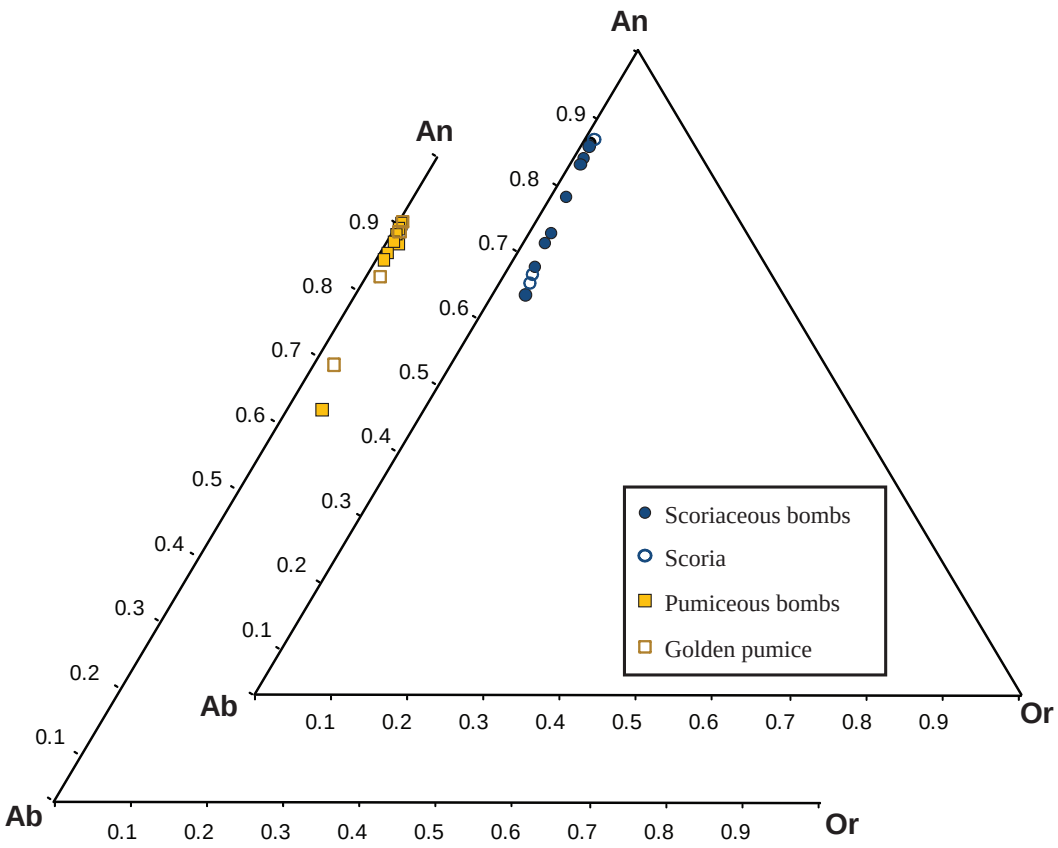

Figure 7. Plagioclase in the pumiceous bombs has complex zoning and high An content (like with plagioclase in the golden pumice; Francalanci et al., 2004). Plagioclase in the scoriaceous bombs also has complex zoning but are not as anorthitic as plagioclase from the pumiceous bombs (like published analyses of plagioclase in scoria; Francalanci et al., 2004).

set), which is consistent with the findings of Francalanci et al. (2004) and Metrich et al. (2001).

4.3 Olivine-hosted melt inclusions and matrix glass

Before discussing the results from our melt inclusion analyses, it is important to note some of the inherent weaknesses of any melt inclusion study. A major goal of most melt inclusion studies is to better understand the volatile concentration in the melt at the time of melt inclusion formation. However, there are several natural processes that could decrease or increase the volatile concentration in the melt inclusion, making it no longer the same composition as the melt. Diffusive exchange of hydrogen between the melt inclusion and the melt can cause H_2O to decrease in the melt inclusion (Danyushevskey et al., 2002), whereas crystallization of the host mineral along the inclusion walls can actually increase volatile concentrations. While the effects of diffusive exchange cannot be corrected, secondary crystallization can sometimes be corrected, especially in olivine. Each melt inclusion was corrected and only a maximum of 10% crystallization of olivine along the inclusion wall occurred. However, the melt inclusions in clinopyroxene experienced much more secondary crystallization, and its effects will be discussed later on.

Another possible way that the melt inclusions could record higher volatile concentrations than the corresponding melt is through diffusive fractionation a a melt inclusion forms, as described by Baker et al. (2008). As a mineral grows, the elements compatible with the mineral will become depleted and the elements incompatible with the mineral will become enriched in the melt directly adjacent to the growing mineral. Any melt inclusions formed from this locally altered melt will record higher volatile

concentrations than the true melt ever contained. The effects of this process cannot be corrected, and so it must be assumed that this process did not occur in order to make any conclusions from the volatile data.

Leakage through fractures or other pathways can also decrease volatile concentrations. Both non-fractured and a few fractured melt inclusions were included in the data set. The compositions of the fractured inclusions show no noticeable differences from the nonfractured melt inclusions. The assumption was made that the fractures occurred after cooling.

Melt inclusions and matrix glass from pumiceous bombs are members of the shoshonite series (Table 4 and 5; Fig. 8; full datasets can be found in Appendices 8.7 and 8.8) and range from potassic trachybasalt to shoshonite (Fig. 8). Melt inclusions and matrix glass from scoriaceous bombs are more homogeneous and are members of the shoshonite series (Fig. 8) According to IUGS classification, they are generally shoshonites (Fig. 8).

4.3.1 Glass chemistry of pumiceous bombs

The olivine-hosted melt inclusions in the pumiceous bombs are bimodal in terms of MgO with one group ranging from 4.27 to 5.77 wt. % and the other group ranging from 2.69 to 3.46 wt. % (Fig. 9). Both groups are on the shoshonite trend (Fig. 8;). However, the MgO-rich melt inclusions are potassic trachybasalts, whereas the melt inclusions with less MgO are shoshonites (Fig. 8). The high-MgO melt inclusions also contain more CaO (11.02-9.67 wt. %) and Al_2O_3 (16.32-17.24 wt. %), and they contain less K_2O (2.40-2.98 wt. %), SiO_2 (48.33-51.41 wt. %), and FeO (7.44-9.40 wt. %) than the low-MgO melt inclusions (Fig. 9). The MgO-poor melt inclusions contain less CaO

Table 4. Selected olivine melt inclusions from pumiceous and scoriaceous bombs

Pumiceous bombs

	strom1 olv1m1	strom1 olv11m3	strom1 olv12m1	strom5 olv3m1	strom5 olv8m1	strom5 olv1m1
SiO_2	50.78	50.55	49.24	52.94	50.82	52.56
TiO_2	1.01	0.90	0.94	1.70	1.84	1.58
Al_2O_3	18.84	18.38	18.66	15.84	15.85	16.17
FeO_{total}	7.11	7.60	8.41	10.34	10.59	9.65
MnO	0.17	0.16	0.18	0.24	0.20	0.22
MgO	1.40	2.43	3.64	2.03	1.98	2.53
CaO	11.96	11.71	11.39	8.21	8.97	7.88
Na_2O	3.89	3.04	2.80	3.63	3.39	3.12
K_2O	3.02	2.67	2.50	4.23	4.05	4.61
P_2O_5	0.76	0.74	0.63	1.16	1.21	1.24
S	0.133	0.133	0.128	0.032[a]	0.069	0.008[a]
Cl	0.183	0.206	0.179	0.178	0.155	0.125
Total	99.34	98.60	98.78	100.51	99.16	99.66
Host olivine						
Fo mol %	81.25	82.39	82.14	70.49	70.18	70.19
SiO_2	39.14	39.20	38.08	36.699	37.735	37.018
MgO	42.81	43.40	43.50	35.311	35.095	35.503
FeO	17.63	16.55	16.84	26.366	26.536	26.894
MnO	0.30	0.29	0.29	0.495	0.487	0.474
CaO	0.27	0.28	0.25	0.352	0.346	0.328
Recalculated compositions[b]						
SiO_2	50.00	49.65	48.33	52.27	50.18	52.32
TiO_2	0.98	0.83	0.88	1.63	1.75	1.56
Al_2O_3	16.95	17.05	17.57	15.19	15.13	15.94
FeO_{total}	7.48	8.22	8.80	11.00	11.30	9.89
MnO	0.13	0.17	0.19	0.25	0.22	0.23
MgO	4.59	5.31	5.68	3.40	3.46	2.99
CaO	9.67	10.88	10.73	7.88	8.57	7.77
Na_2O	3.14	2.82	2.63	3.48	3.23	3.07
K_2O	2.42	2.47	2.35	4.06	3.86	4.54
P_2O_5	0.57	0.68	0.59	1.12	1.15	1.22
S	0.055	0.132	0.125	0.031	0.066	0.007
Cl	0.172	0.191	0.168	0.171	0.147	0.123
Total	96.20	98.55	98.19	100.47	99.13	99.64
S/Cl	0.32	0.69	0.74	0.18	0.45	0.06
X_{fo}[c]	0.04	0.08	0.06	0.04	0.05	0.01

[a] S concentration is below detection limits; see text

[b] Melt inclusions recalculated after Luhr, 2001

[C] The fraction of post-entrapment crystallization of olivine

Table 4. cont.

Scoriaceous bombs

	strom07-1 olv2m1	strom07-1 olv3m1	strom07-2 olv2m1	Strom07-2 olv4-m2	strom07-5 olv1m1	strom07-5 olv4m2
SiO_2	51.28	48.41	53.30	54.45	53.70	52.91
TiO_2	1.29	1.80	1.50	1.44	1.64	1.78
Al_2O_3	16.57	15.01	15.16	14.72	15.36	15.81
FeO_{total}	10.13	11.33	9.91	9.95	9.76	10.17
MnO	0.14	0.24	0.22	0.20	0.16	0.25
MgO	2.66	2.78	3.41	3.22	2.46	2.41
CaO	9.68	11.13	7.39	7.22	8.28	8.63
Na_2O	3.02	2.35	3.45	3.48	3.58	3.25
K_2O	3.51	3.63	4.31	4.23	4.19	3.94
P_2O_5	0.80	2.40	0.32	0.36	1.15	1.11
S	0.038[a]	0.019[a]	0.012[a]	0.005[a]	0.012[a]	0.004[a]
Cl	0.123	0.334	0.109	0.115	0.136	0.107
Total	99.26	99.38	99.07	99.37	100.41	100.35
Host olivine						
Fo mol %	73.83	72.19	73.07	72.72	72.71	72.32
SiO_2	38.382	37.745	36.72	36.80	37.04	38.48
MgO	37.082	36.3	37.01	37.04	36.86	35.92
FeO	23.435	24.923	24.34	24.77	24.64	24.46
MnO	0.415	0.461	0.49	0.46	0.48	0.45
CaO	0.368	0.335	0.34	0.31	0.32	0.32
Recalculated compositions[b]						
SiO_2	50.73	48.00	53.12	54.24	53.03	52.32
TiO_2	1.24	1.74	1.48	1.42	1.57	1.70
Al_2O_3	15.90	14.49	15.01	14.54	14.74	15.16
FeO_{total}	10.65	11.78	10.05	10.12	10.36	10.75
MnO	0.15	0.25	0.22	0.21	0.17	0.26
MgO	4.04	3.92	3.74	3.61	3.83	3.79
CaO	9.30	10.75	7.32	7.14	7.97	8.29
Na_2O	2.90	2.27	3.41	3.44	3.44	3.11
K_2O	3.37	3.50	4.27	4.18	4.03	3.78
P_2O_5	0.77	2.31	0.31	0.35	1.11	1.06
S	0.036	0.019	0.011	0.005	0.011	0.004
Cl	0.118	0.322	0.108	0.114	0.131	0.103
Total	99.23	99.30	99.05	99.35	100.38	100.32
S/Cl	0.31	0.06	0.11	0.05	0.08	0.00
X_{fo}[c]	0.04	0.04	0.01	0.01	0.04	0.04

[a] S concentration is below detection limits; see text

[b] Melt inclusions recalculated after Luhr, 2001

Table 5. Selected matrix glass from pumiceous and scoriaceous bombs

Pumiceous bombs

	strom1 gls	strom1 gls	strom1 gls	strom5 gls	strom5 gls	strom5 gls
SiO_2	51.25	50.18	49.93	49.01	50.25	49.72
TiO_2	0.92	0.91	0.86	0.95	1.00	0.95
Al_2O_3	17.74	17.65	18.07	17.77	18.07	18.27
FeO_{total}	7.94	8.27	7.84	8.10	8.40	8.28
MnO	0.24	0.04	0.13	0.20	0.16	0.17
MgO	5.34	5.77	5.32	6.45	5.82	5.86
CaO	9.97	10.39	9.97	11.62	11.57	11.85
Na_2O	3.10	2.97	2.74	2.53	2.43	2.47
K_2O	2.64	2.40	2.81	2.05	2.01	1.95
P_2O_5	0.60	0.71	0.64	0.76	0.66	0.68
S	0.06	0.04	0.02[a]	0.02[a]	0.03[a]	0.01[a]
Cl	0.14	0.14	0.13	0.10	0.11	0.10
Total	99.97	99.46	98.43	99.55	100.50	100.29
S/Cl	0.43	0.31	0.13	0.21	0.24	0.11

Scoriaceous bombs

	strom07-1 gls	strom07-1 gls	strom07-2 gls	strom07-2 gls	strom07-5 gls	strom07-5 gls
SiO_2	53.76	53.12	54.27	53.66	53.31	54.32
TiO_2	1.44	1.44	1.51	1.45	1.50	1.47
Al_2O_3	15.32	15.60	15.30	15.16	15.66	15.54
FeO_{total}	8.97	9.96	9.38	9.97	9.51	9.69
MnO	0.15	0.22	0.27	0.18	0.12	0.17
MgO	2.69	3.34	3.32	3.44	3.39	3.36
CaO	8.92	6.64	7.24	7.42	7.37	7.49
Na_2O	3.37	3.55	3.84	3.38	3.30	3.12
K_2O	4.30	4.66	4.38	4.16	4.45	4.54
P_2O_5	0.37	0.94	0.31	0.94	1.05	1.00
S	0.01[a]	0.00[a]	0.01[a]	0.01[a]	0.02[a]	0.00[a]
Cl	0.12	0.13	0.11	0.11	0.12	0.13
Total	99.40	99.57	99.93	99.86	99.77	100.80
S/Cl	0.10	0.00	0.09	0.11	0.13	0.00

[a] S concentration is below detection limits; see text

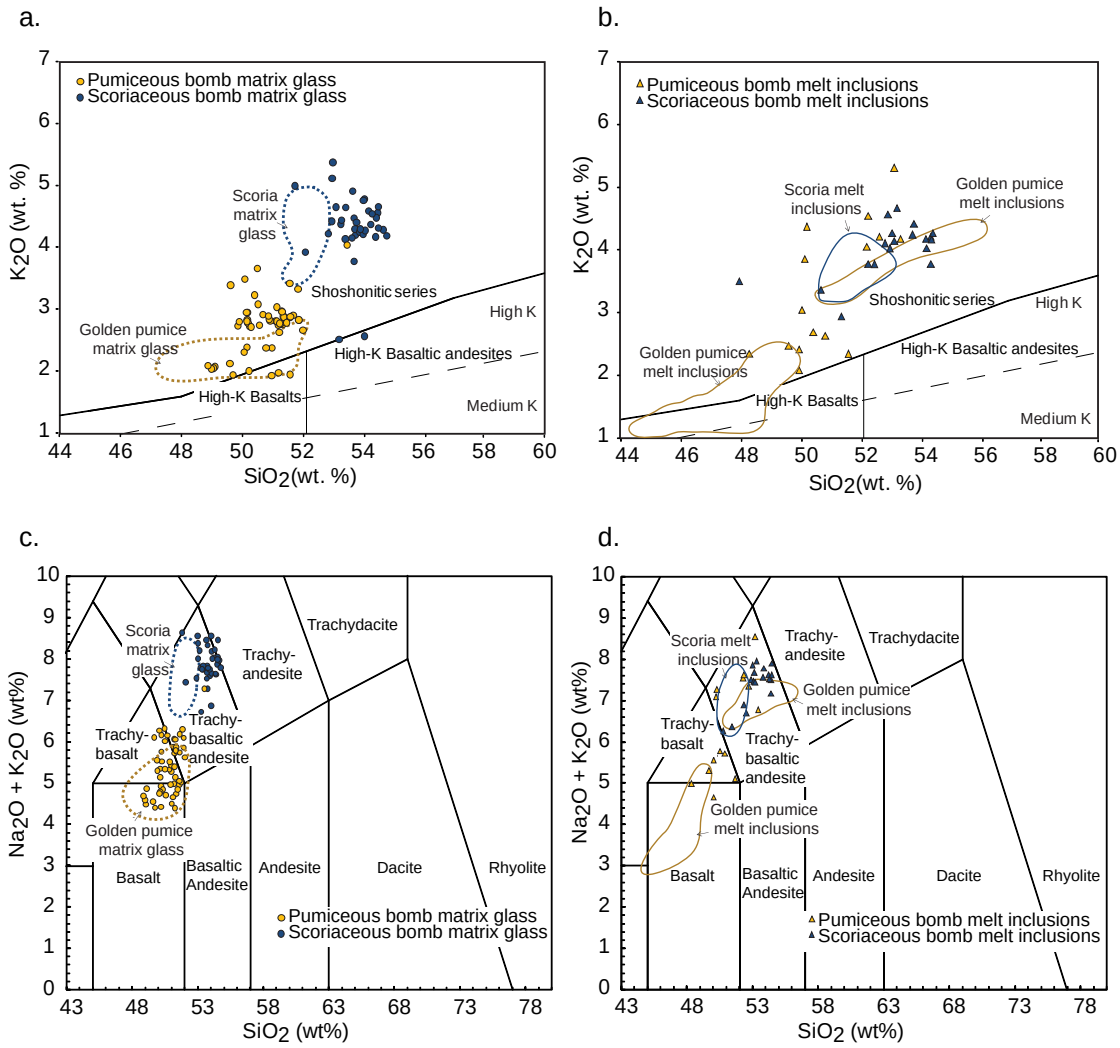

Figure 8. SiO_2 v K_2O (a. and b. after Francalanci et al., 2004) and IUGS (c. and d.) diagrams of melt inclusions and matrix glass. a. The matrix glass in the pumiceous bombs is generally shoshonitic, although a few analyses plot in the high-K basalt field. The scoriaceous matrix glass is shoshonitic as well but is higher in SiO_2. b. The melt inclusions in both the pumiceous bombs and scoriaceous bombs are shoshonitic, but the scoriaceous melt inclusions are higher in SiO_2. c. According to IUGS classifications, the matrix glass in the pumiceous bombs ranges from basalt to trachybasaltic andesite. The matrix glass from the scoriaceous bombs is generally trachybasaltic andesite. d. The pumiceous melt inclusions range from basalt to trachybasaltic andesite. The melt inclusions from the scoriaceous bombs are trachybasaltic andesite field.

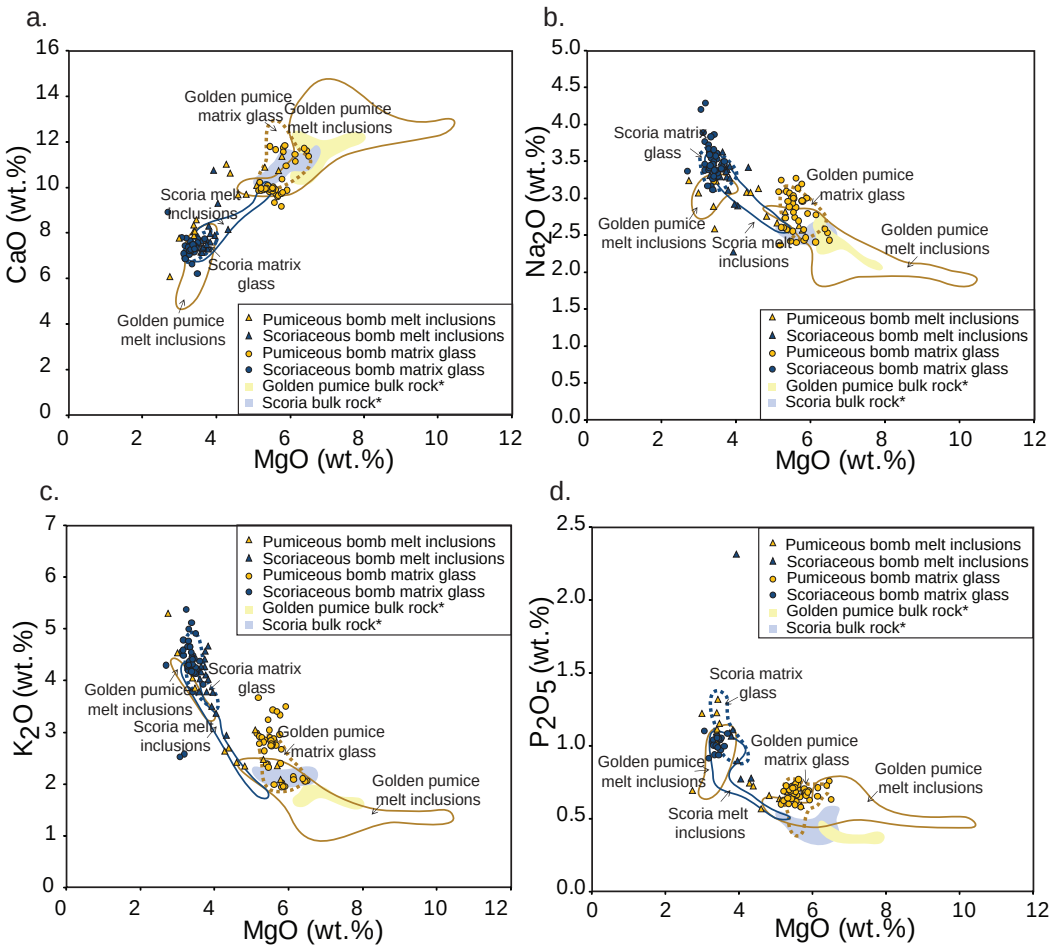

Figure 9. Variations diagrams of major elements in olivine-hosted melt inclusions and matrix glass from pumiceous and scoriaceous bombs. a. The pumiceous bombs contain melt inclusions and melt inclusions that are generally richer in MgO and CaO than the scoriaceous bombs. However, a few melt inclusions from the pumiceous bombs are compositionally more similar to the scoriaceous bombs. b. Melt inclusions and matrix glass from the pumiceous bombs generally contain smaller concentrations of Na2O than the scoriaceous bombs. c. K2O concentrations are generally higher in melt inclusions and matrix glass in the scoriaceous bombs than the pumiceous bombs. d. The pumiceous bombs contain melt inclusions and matrix glass that are generally poorer in P2O5 than the scoriaceous bombs.

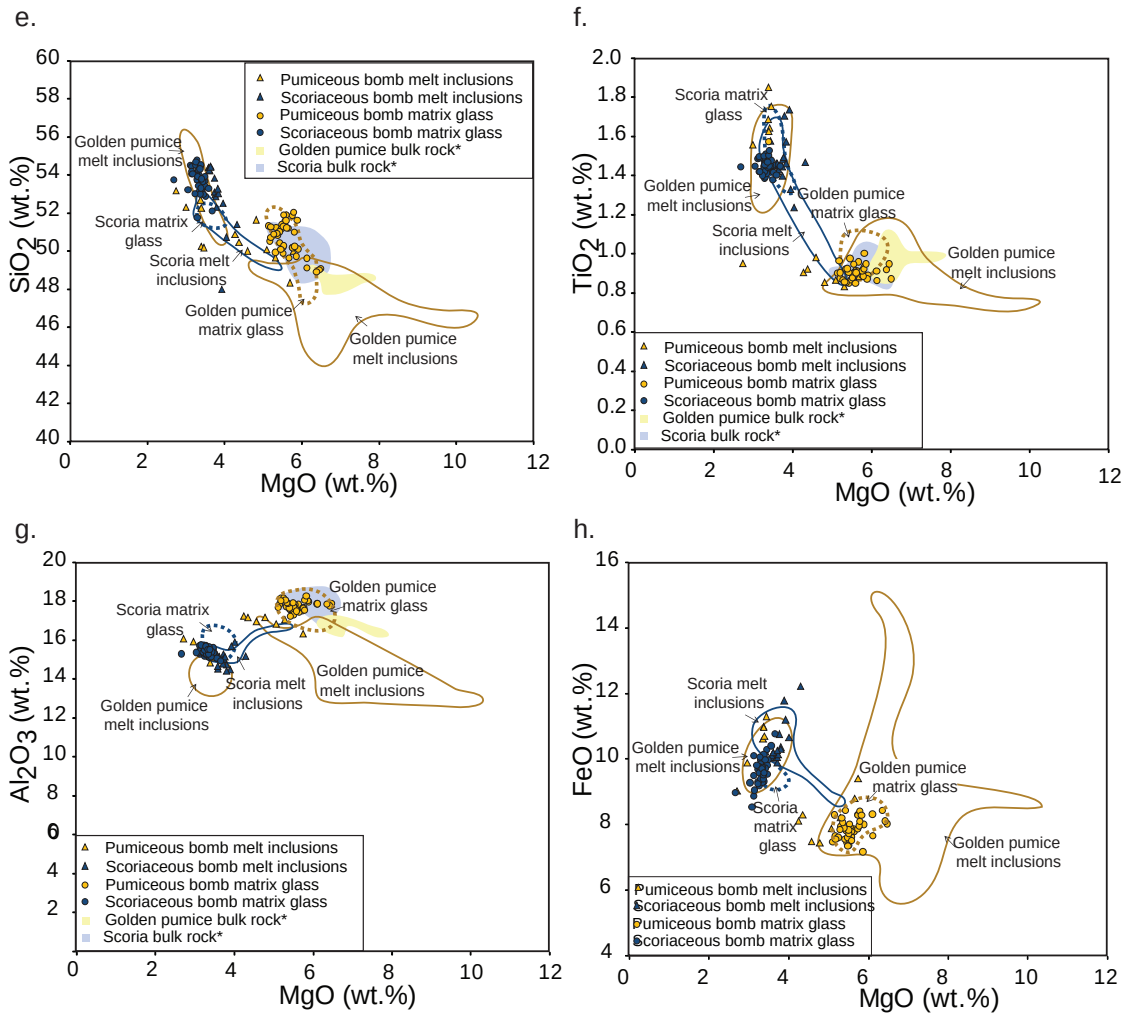

Figure 9 cont. e. Melt inclusions and matrix glass from the pumiceous bombs generally contain smaller concentrations of SiO2 than the scoriaceous bombs. f. TiO2 concentrations are generally higher in melt inclusions and matrix glass in the scoriaceous bombs than the pumiceous bombs. g. The pumiceous bombs contain melt inclusions and melt inclusions that are generally richer in Al2O3 than the scoriaceous bombs. h. FeO concentrations are generally higher in melt inclusions and matrix glass in the scoriaceous bombs than the pumiceous bombs.

(6.08-8.34 wt. %), and Al_2O_3 (14.86-16.09 wt. %), and they contain more K_2O (3.86-5.31 wt. %), SiO_2 (50.18-53.19 wt. %), and FeO (9.04-11.30 wt. %) (Fig. 9). The gap between the two melt inclusion groups is also apparent in volatile concentrations (Fig. 10). Before discussing these concentrations, the detection limit for S should be addressed. The stated detection limit for S using the analytical conditions described above is .0399. However, a statistical two-tailed T-test indicates that there is some statistical value to the concentrations that are below the detection limit, and thus, they will still be discussed but will be marked with a *.

The MgO-rich melt inclusions have more S (0.05-0.13 wt. %) than the MgO-poor olivines (.004* -0.07 wt. %). There is a smaller difference in Cl. The MgO-rich melt inclusions have Cl concentrations from 0.08-0.19 wt. %, whereas the MgO-poor melt inclusions contain Cl concentrations of 0.13-0.17 wt. %. The two groups of melt inclusions are hosted by compositionally different olivine grains. The MgO-rich melt inclusions are hosted by olivine that is more primitive (Fo_{78-82}) than the olivine that hosts the MgO-poor melt inclusions (Fo_{70-71}; Fig. 11).

The matrix glass (Table 5) from the pumiceous bombs ranges from the high-K to the shoshonite series (Fig. 8). According to IUGS classification, they are shoshonites. There are several differences between the matrix glass and the melt inclusions in the pumiceous bombs. First, although there is some overlap, the matrix glass has higher MgO concentrations (5.14-6.45 wt. %) than many of the melt inclusions (2.69-5.77 wt. %) (Fig. 9). Normally, in a closed, evolving magma system, crystallization of olivine and pyroxene would decrease the amount of MgO in the residual melt. The matrix glass should have less MgO than any melt inclusions trapped earlier in the evolution of the

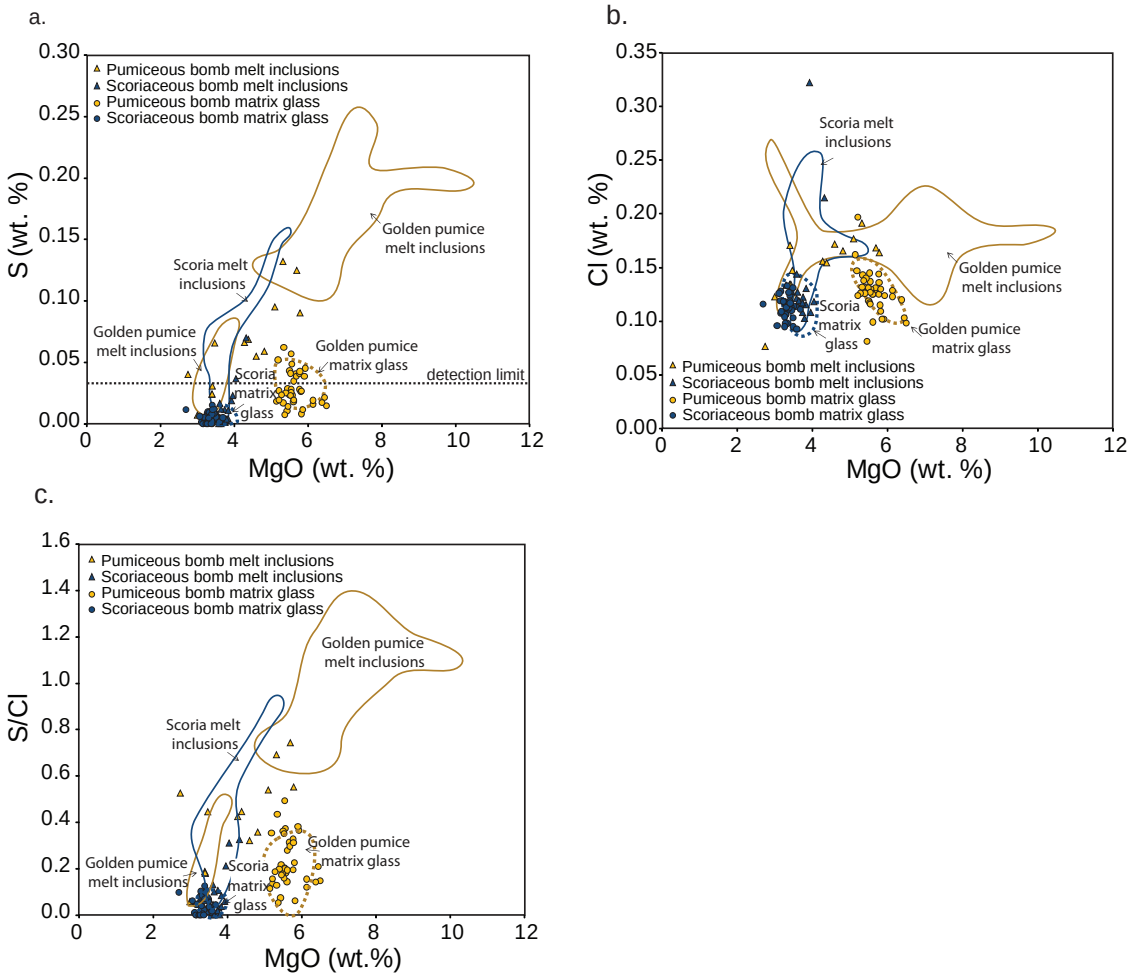

Figure 10. Scatter diagrams of MgO and volatiles in glassy components of ejecta from Stromboli Volcano. a. The pumiceous bombs are richer in sulfur than the scoriaceous bombs as well. b. The pumiceous bombs contain only slightly higher concentrations of chlorine than the scoriaceous bombs. c. The difference in volatile content, especially in sulfur, is also evident in the S/Cl ratio. The pumiceous bombs have a significantly higher S/Cl ratio (especially in the melt inclusions) than the scoriaceous bombs.

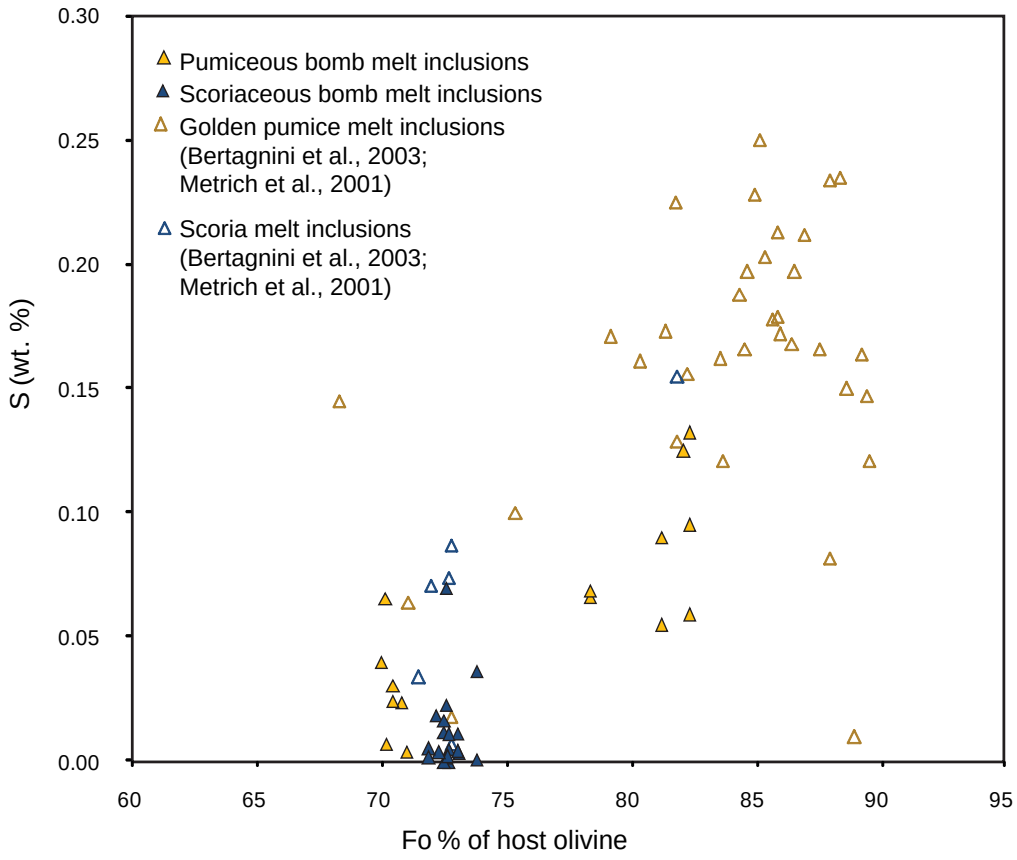

Figure 11. Fo % of host olivine versus sulfur content of melt inclusion. The two groups of melt inclusions in the pumiceous bombs have different sulfur content as well as different Fo content in their host olivine. The amount of S is loosely correlated with the Fo content of the host olivine. Melt inclusions with more sulfur are hosted by more primitive olivines (Fo78-82). More evolved olivines (Fo70-71) contain melt inclusions with smaller sulfur concentrations. The scoriaceous bombs contain one olivine group with melt inclusions that contain similar concentrations of sulfur.

magma. This is not the case for the pumiceous bombs, however. Magma mixing is a likely explanation for the elevation of MgO in the matrix glass. The influx of a more primitive, MgO-rich magma prior to eruption could cause the matrix glass to be more MgO-rich than the melt inclusions. This process could also explain the reversely zoned olivine and clinopyroxene in the pumiceous bombs.

Differences between the melt inclusions and matrix glass are also seen in sulfur and chlorine concentrations (Fig. 10). In the pumiceous bombs, the melt inclusions have variable S concentrations at a maximum of 0.13 wt. % and Cl concentrations at a maximum of 0.19 wt. %. The matrix glass varies from 0.01* wt. % to 0.06 wt. % in S and 0.12 wt. % to 0.2 wt. % in Cl. If the olivine-hosted melt inclusions have remained closed, the pumiceous bombs potentially lost from 57% (0.07 wt. %) to as much as 100% (0.13 wt. %) of the original S dissolved in the magma by the time the matrix glass in the bombs completely cooled and partially degassed. Additionally, 0% (0.0 wt. %) to as much as 42% (0.08 wt. %) of the Cl could also have been lost. These differences between melt inclusions and matrix glass are also reflected in the S/Cl ratio. The melt inclusions have a maximum ratio of 0.74 wheras the matrix glass has a more variable S/Cl ratio that ranges from 0.49 to 0.24. This means that S was more efficiently degassed than Cl.

4.3.2 Glass chemistry of scoriaceous bombs

The olivine melt inclusions from the scoriaceous bombs lie on the shoshonite trend (Fig. 8; classification according to SiO_2 vs K_2O) and are dominantly shoshonites (classification according to IUGS). The scoriaceous matrix glass also lies on the shoshonite trend and ranges from shoshonite to latite.

The matrix glass (Table 5) and olivine-hosted melt inclusions (Table 4) from the scoriaceous bombs are generally similar to each other. The majority of melt inclusions overlap in composition with the matrix glass for all major elements (Fig. 9). Some of the melt inclusions, however, have slightly higher CaO concentrations (maximum 10.75 wt. % for melt inclusions compared to 8.92 wt. % for matrix glass), and FeO concentrations (maximum 12.23 wt. % for melt inclusions compared to 10.77 wt. % for matrix glass) concentrations and slightly lower Na_2O concentrations (minimum 2.27 wt. % for melt inclusions compared to 3.15 wt. % for matrix glass), K_2O concentrations (minimum 2.94 wt. % for melt inclusions compared to 3.85 wt. % for matrix glass), and SiO_2 concentrations (minimum 50.00 wt. % for melt inclusions compared to 51.74 wt. % for matrix glass).

Volatile concentrations in the melt inclusions and matrix glass of the scoriaceous bombs are fairly similar as well (Fig. 10). The majority of melt inclusions from the scoriaceous bombs record sulfur concentrations from 0.00* wt. % to 0.02* wt. % and chlorine concentrations from 0.10 wt. % to 0.14 wt. %. Two anomalous melt inclusions record S concentrations as high as 0.06 wt. % and Cl concentrations as high as 0.32 wt. %. Matrix glass records sulfur concentrations from 0.00* wt. % to 0.02* wt. % and chlorine concentrations varying from 0.14 wt. % to 0.09 wt. %. Neglecting the two anomalous melt inclusions, the scoriaceous bombs would have potentially lost a maximum of 64% (0.05 wt. %) of the Cl and a maximum of 100% (0.02 wt. %) of the S originally in the magma as the bomb degassed. The S/Cl ratio is very similar as well, with most melt inclusions and matrix glass plotting at 0.6 or less.

The primitive olivine-hosted melt inclusions and matrix glass from the pumiceous bombs are more MgO-rich and more volatile-rich than melt inclusions from the scoriaceous bombs (Fig. 10). Specifically, the pumiceous bombs contain melt inclusions with a maximum 0.13 wt. % more sulfur than the scoriaceous bombs. This indicates that the pumiceous bombs originated from a more primitive, less degassed magma source.

It is important to note that the sulfur concentrations of the melt inclusions from the pumiceous bombs (b.d.l.- 0.13 wt. % S) are on the low end of the range documented by Bertagnini et al. (2003) and Metrich et al. (2001) in golden pumice samples (0.00-0.25 wt. % S; Fig. 10). There are several possible reasons for this. The first is inherent differences in the empirical methods used in the analysis of the melt inclusions. Bertagnini et al. (2003) and Metrich et al. (2001) used a 10nA beam current, 10 μm beam size and 10-15 s counting times on major elements, and 40 nA, 15μm and 120s for Cl, S, and P. In contrast, in this study, every element was analyzed using a 10 nA beam current, 10 μm beam size and 20 s counting times. Differences in calibration standards used could also cause the difference.

Alternatively, a difference in the degree of magma evolution could also cause the pumiceous bombs to be poorer in sulfur. The pumice clasts analyzed by Bertagnini et al. (2003) and Metrich et al. (2001) were small fragments collected from ash layers on the flank of Stromboli. These small rock fragments came from explosive, volatile-rich eruptions, and thus they contain primitive olivine with volatile-rich melt inclusions. The pumiceous bombs were large fragments from the top of the volcano. It is possible that the bombs were ejected from a less volatile-rich (partially degassed, more evolved) and thus less energetic eruption. Evidence for a more evolved magma include less CaO and MgO

in melt inclusions from the pumiceous bombs (6.08-11.36 wt. % and 2.73-5.77 wt. % respectively) than the melt inclusions from golden pumice studied in the past (CaO: 4.80-14.36 wt. % ; MgO: 3.02-7.84 wt. %) (Fig. 9). This should explain why the bombs were larger fragments and were not ejected far from the vent. It would also explain why the olivines in the pumiceous bombs are not quite as primitive as those analyzed by Bertagnini et al. (2003) and Metrich et al. (2001). It is harder to explain the lack of a difference in chlorine using this idea, however. Oxidixed sulfur is less soluble in the melt than chlorine, so it is possible that as the open-system magma evolved and degassed at depth, sulfur was lost more efficiently than chlorine.

Magma mixing could also lower the amount of S in the magma. It is acknowledged that the volatile-rich (golden pumice) magmas and degassed (scoria) magmas mix at least to some extent before eruption (Francalanci et al., 2004). If the pumiceous bombs originated from a magma mixed with a larger component of the degassed magma than golden pumice studied previously, this would effectively dilute the S-concentrations in the pumiceous bombs.

4.4 Estimate of H_2O concentration in pumiceous bombs

Because of the complete lack of sulfides in the glass or enclosed in minerals, it appears that sulfides may never have been present in either magma. This would mean that the magmas were sulfide undersaturated. With this assumption, an estimate of water concentration in the pumiceous bombs can be made, using the sulfide saturation model of Liu et al. (2007). Assuming a pressure of 270 MPa and a temperature of 1150 ºC (di Carlo et al., 2006), the maximum water concentration that would still produce sulfide saturation values above S concentrations analyzed is ~1.5 wt. % H_2O. Published water

concentrations (Bertagnini et al., 2003; Metrich et al., 2001) as well as experimental studies of the golden pumice (di Carlo et al., 2006) indicate that the slightly less evolved golden pumice contains water concentrations ~2.6 wt. % . This means that the more evolved pumiceous bombs contain not just less S, but also at least 1 wt. % less H_2O.

4.5 Clinopyroxene-hosted melt inclusions

The melt inclusions in clinopyroxene have distinctly different compositions from the corrected olivine melt inclusions (Table 6; Fig. 12). This offset appears to be caused by post-entrapment crystallization of clinopyroxene along the melt inclusion walls. The secondary crystallization enriches the melt inclusions in elements incompatible in the clinopyroxene, such as K_2O and volatiles. The melt inclusions are also depleted in elements such as CaO and MgO, which are compatible in clinopyroxene.

The enrichment of incompatible elements is easily seen in a CaO vs K_2O plot in Figure 12. If it is assumed that the original clinopyroxene melt composition was similar to the most primitive olivine-hosted melt inclusions (~2.0 wt. % K_2O), then K_2O at least doubled to a minimum of ~4.5 wt. %, likely due to secondary crystallization. Using this line of reasoning, 50-75% post-entrapment crystallization could have occurred. This much crystallization would at least double volatile concentrations as well, so it was determined that the pyroxene melt inclusions are probably too affected by secondary crystallization to constrain the original composition of the melt.

4.6 Sulfur variations in matrix glass near vesicles

Elemental concentration maps of glass near vesicles were created using an electron microprobe. Maps for sulfur and major elements Fe, Al, and Si are included in Appendix 8.8. Slight variations are evident in the sulfur map, but these variations are not

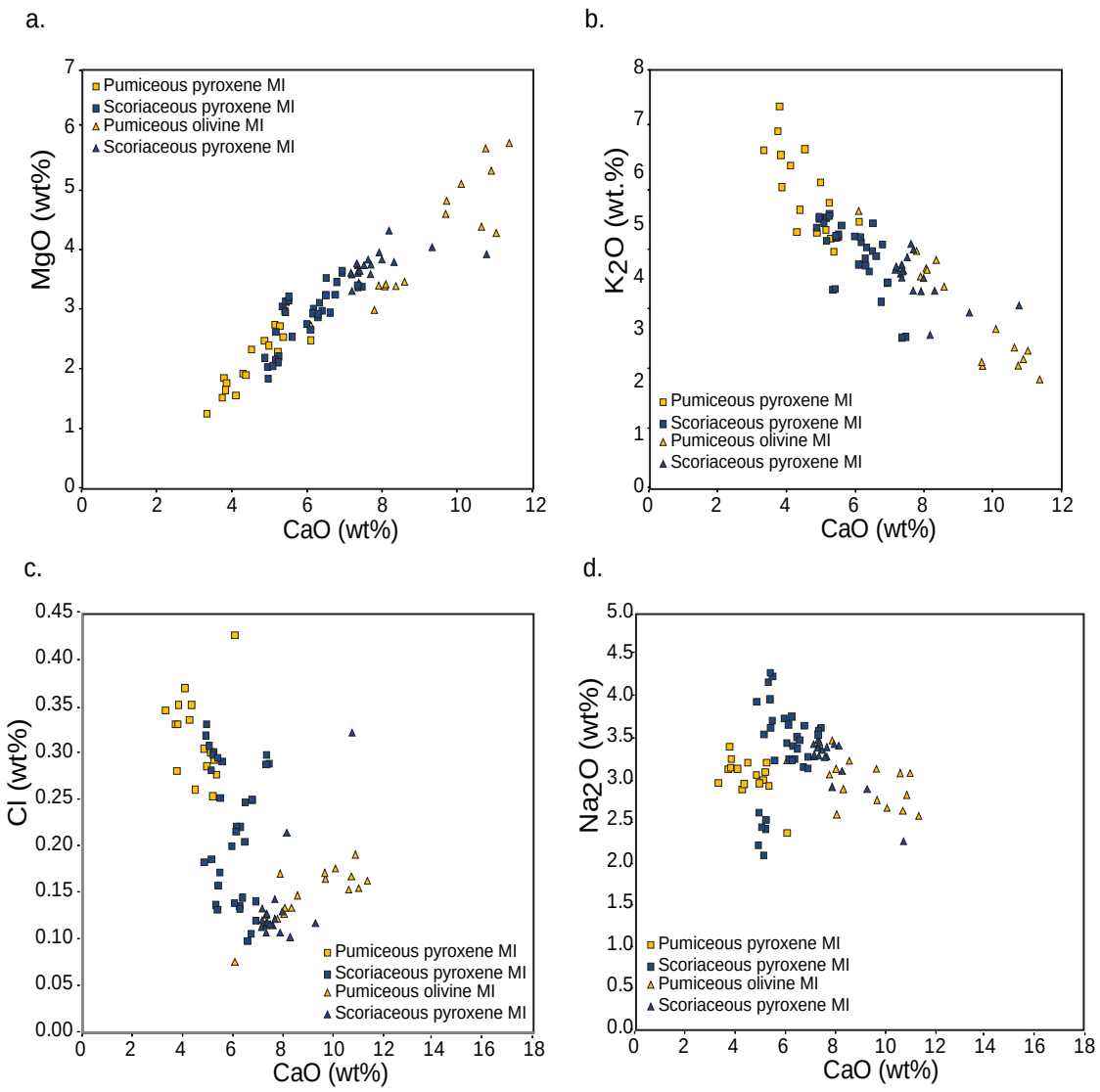

Figure 12. Scatter diagrams comparing corrected olivine melt inclusions with pyroxene melt inclusions. a. Due to secondary crystallization, the clinopyroxene melt inclusions are depleted in CaO and MgO, which are compatible in clinopyroxene. b,c,d. K2O, Cl, and Na2O are enriched in the clinopryoxene melt inclusions because these elements are incompatible in clinopyroxene.

apparent in the major element maps. Sulfur maps were also made at a smaller scale in some areas (Fig. 13). Variations in sulfur can be seen more clearly at these scales. They form streaks or bands that are commonly parallel to the vesicle margins, but some bands intersect the vesicle. These variations in sulfur mimic the flow fabric seen in the glass in plane-polarized light under a petrographic microscope.

4.7 Physical description of metal alloys

In reflected light, the metal alloys are a yellow-gold color and are highly reflective (Fig. 14). They range in size from a few microns to a maximum of 150 µm. The metal alloys commonly have a characteristic cockscomb structure, and the larger alloys have slight color variations that could reflect compositional variation. They are never found in the matrix glass, but almost always in vesicles found in both glassy and crystallized matrix. Some of these vesicles are inflated, with even thinner, more oblong vesicles surrounding them. These smaller vesicles were deformed as the inflating vesicle grew before and after emplacement.

Rarely, the alloys are in concentric fractures surrounding the vesicles (Fig. 14). This could indicate that fractures are the pathway through which the metals are transported to the vesicle or the metal alloy-filled fractures could simply be areas where the metal-rich gases leaked out of the vesicle. The alloy grains are commonly found directly adjacent or attached to the vesicle wall and the curvature of the alloy matches that of the nearby vesicle wall. This suggests that the alloys originally were attached to the vesicle wall and grew into the interior of the vesicle. Due to shrinkage during cooling or during sample collection and preparation, however, they became detached from the wall (Hunter et al., 2007).

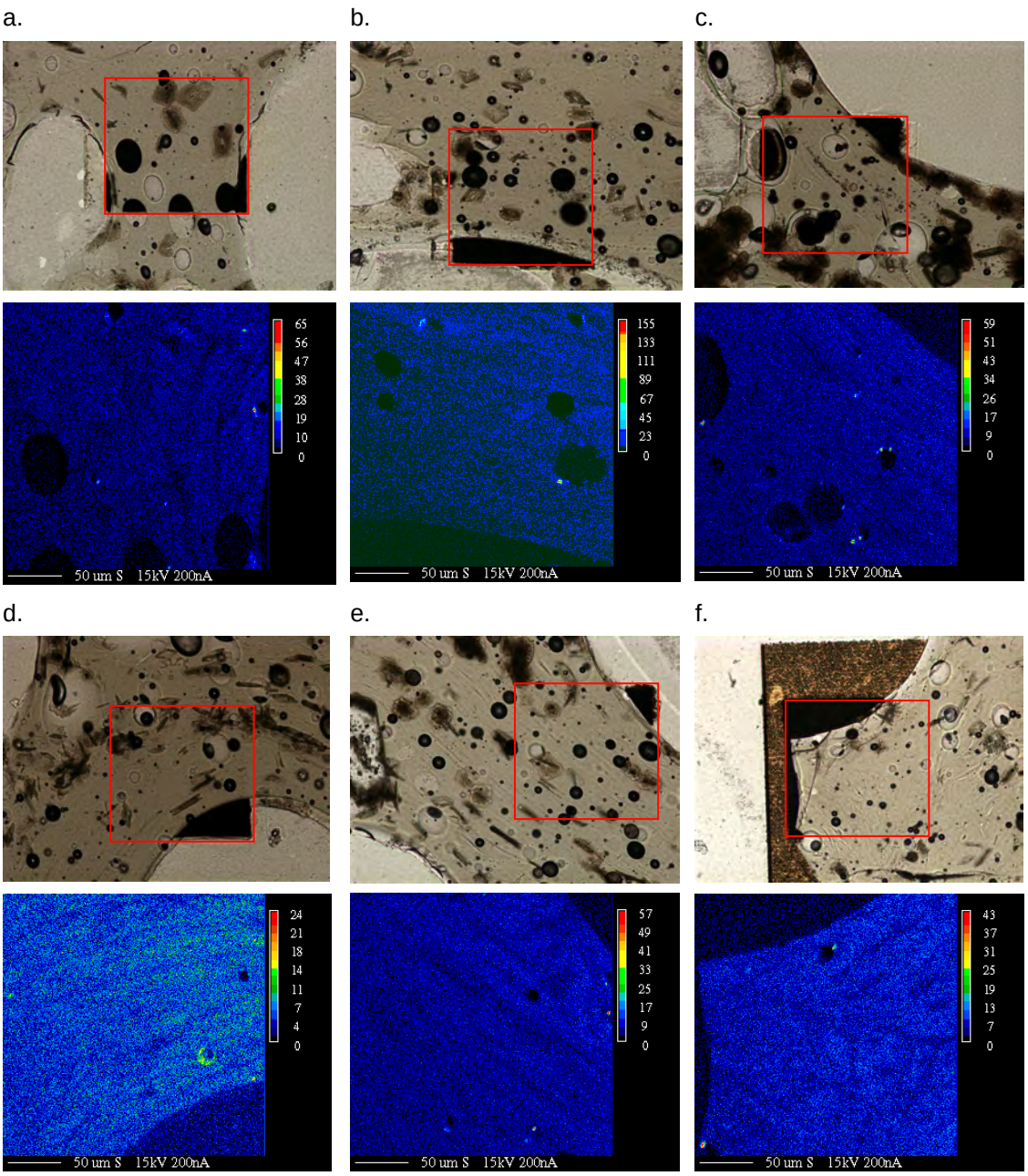

Figure 13. Photomicrographs of glass next to vesicles with corresponding sulfur maps a. Banding in sulfur concentrations can be seen running parallel to the vesicle to the right of the image. b. More sulfur banding following the shape of the large vesicle at the bottom of the image. c. The sulfur variations commonly mimic flow textures seen in the glass in plane-polarized light. d. More variation that mimics flow variations. e. Locally, the flow variations intersect the vesicles, and this can also be seen in the sulfur banding. f. The sulfur banding intersects the vesicle through chaotic flow textures in the glass.

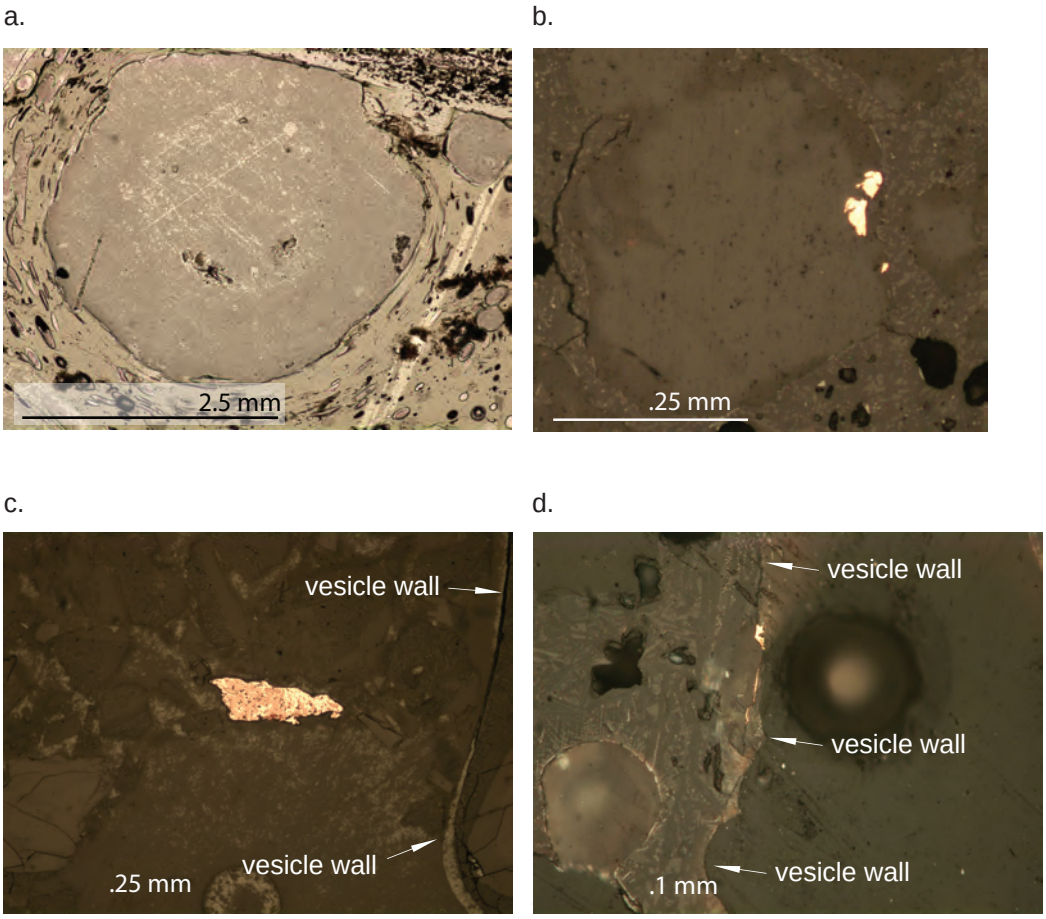

Figure 14. Images of metal alloys in reflected light. a. Metal alloy grains are commonly found in inflated vesicles like this one. The inflated vesicles are fairly round and are commonly surrounded by smaller vesicles deformed as the inflated vesicle grew. b. Metal alloy grain with common 'cockscomb' structure. The convex surfaces of the alloys follow the contours of the vesicle walls. c. Metal alloy with heterogeneous composition evident in reflected light. d. Metal alloys are usually found in the vesicles. Rarely, the alloys are found in concentric fractures leading to vesicles, as shown in this image.

There is no evidence of primary magmatic sulfides in the bombs or from previously studied samples of either type erupted during the recent activity (Bertagnini et al., 2003). However, Hunter et al. (2007) documented rare, small vapor-phase sulfides (10 μm or less) on vesicle walls of some of the pumiceous bombs.

Many of the outer surfaces of the alloy grains host vapor-phase sulfides, chlorides, bromides, etc. They are generally too varied and small to characterize via microbeam methods available to us and were beyond the scope of this study.

4.8 Number and size of metal alloys

The size and number of alloy grains were measured in thin sections under reflected light from both the crystallized interior of the bombs and the glassy rind (Fig. 15). The alloy grains range in size from ~2 μm to 150 μm across. The size distributions for the samples are skewed to the right (nonnormal distribution), so the Wilcoxon rank sum test (Keller, 2001) was used to see if the distributions in the more primitive, volatile-rich pumiceous bombs were statistically distinct from the degassed scoriaceous bombs. The test was also used to compare the slowly-cooled, crystallized interior of the bombs to the quenched, glassy rinds.

Although the sample size is small, most sample pairs indicate that there is strong evidence that the pumiceous bombs contain an alloy population that is significantly different from that of the scoriaceous bombs. Specifically, the pumiceous bombs contain more metal alloys of a larger size than the scoriaceous bombs. The crystallized interiors of the bombs contain more alloy grains than the glassy rinds. However, the Wilcoxon rank sum test indicates that there is no evidence that size distributions of the alloy grains from the bomb interiors are statistically different in size from those in the crystallized

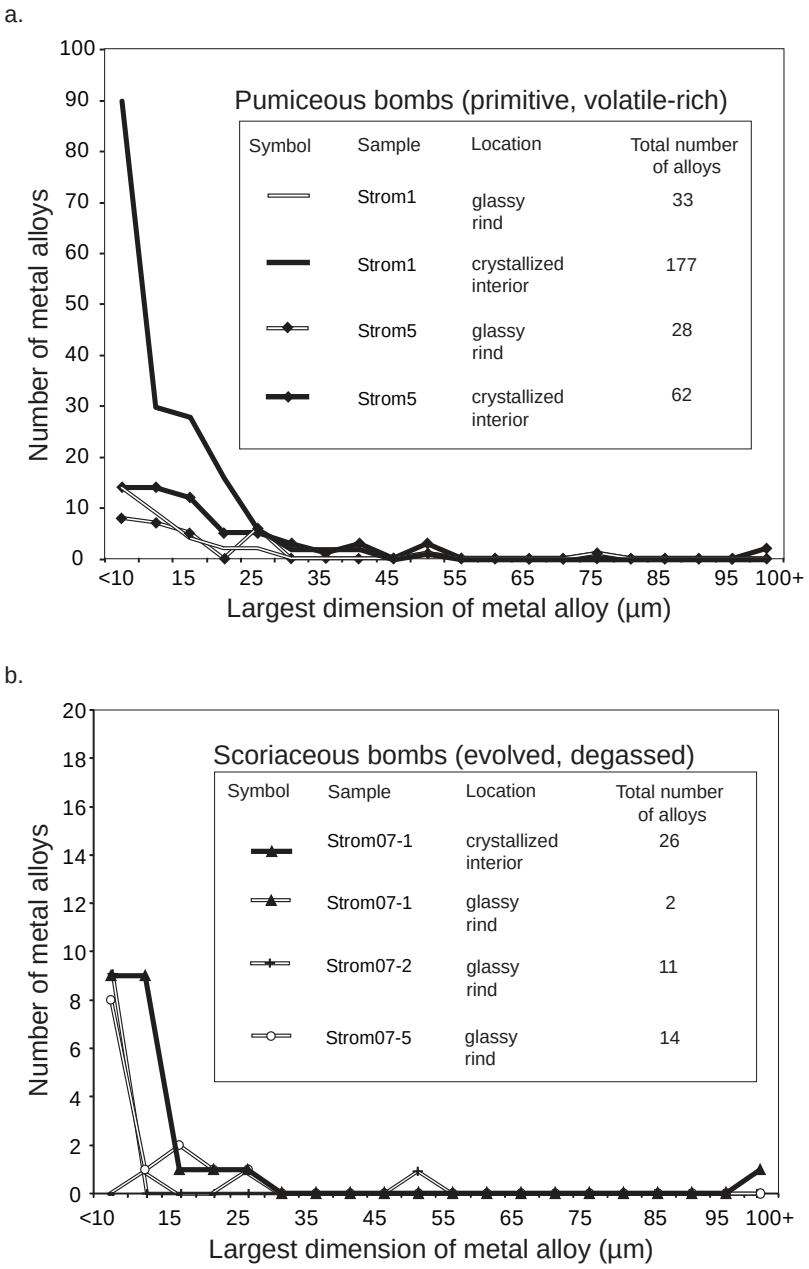

Figure 15. Number of metal alloys according to the largest dimension of the alloy. a. The amount of alloys found in the pumiceous bombs depends on the location inside the bomb. The more slowly-cooled, crystallized interior of the bomb contains more alloys than the quenched glassy rind. b. The amount of alloys found in the scoriaceous bombs again depends on the location inside the bomb. Similar to the pumiceous bombs, the slowly-cooled, crystallized interior of the bomb contains more alloys than the quenched glassy rind. When comparing the same areas of pumiceous bombs to the same areas of the more evolved, degassed scoriaceous bombs (i.e. crystallized interior to crystallized interior or glassy rind to glassy rind), it is apparent that the more primitive, volatile-rich pumiceous bombs contain more alloys of a larger size.

rind. This could mean that the processes forming the metal alloys in the crystallized interior of the bomb are the same as the processes forming metal alloys in the glassy rind. The only difference would be the scale of these processes. The slowly-cooled, crystallized interior may have expelled a greater proportion of volatiles and metals to the vesicles, whereas in the quickly-quenched, glassy rind, volatiles and metals were still trapped in the glass (or escaped along fractures to the surface of the bomb), so that less metals could be transported to the vesicles.

In summary, the data suggests that the number and size of metal alloy grains found in a bomb depends on the location inside the bomb and the type of bomb. The interior of the bombs contain more alloy grains than the glassy exterior. In addition, the petrologically distinct pumiceous bombs (more primitive and more volatile-rich) contain more metal alloy grains of a larger size than the scoriaceous bombs (more evolved and degassed).

5. Discussion

5.1 Possible origins for the pumiceous bombs and scoriaceous bombs

Higher volatile concentrations (especially in sulfur) in both melt inclusions and matrix glass as well as complexly zoned minerals indicate that the pumiceous bombs, though slightly more evolved than typical golden pumice, originated from a primitive magma that was not completely degassed. Reversely zoned olivine and clinopyroxene and variable volatile concentrations in melt inclusions and matrix glass also indicate that these samples were likely influenced by magma mixing. In fact, the more evolved olivine grains that contained melt inclusions with more evolved compositions and less volatiles are very similar to what was found in the scoriaceous bombs. It is possible that the

evolved olivine grains came from the magma that produced the scoriaceous bombs. This would mean that the two magma types mixed. This has been suggested by several prior studies (Francalanci et al., 2004; Landi et al., 2004).

More evolved mineral compositions and lower volatile concentrations indicate that the metal alloy-poor scoriaceous bombs probably came from a magma that was more evolved and relatively degassed.

5.2 The effect of magma trace metal composition on the formation of alloys

The fact that there were only slight or nonexistent differences in trace metals indicates that the pumiceous bombs are not particularly more metal rich than the scoriaceous bombs. The fact that the pumiceous bombs are slightly more sulfur rich is important however. Additionally, other workers, using more samples and different methods, have confirmed the S-rich character of the golden pumice (Bertagnini et al., 2003; Metrich et al., 2001). This could mean that the number of alloys found in the samples is not necessarily controlled by the amount of available metals but actually by the amount of volatiles that are available to complex with and transport the metals.

5.3 The relative importance of S versus Cl in the transport of metals

S is very important in the transport of the metals that compose the alloy grains found in the vesicles. Overall, the pumiceous bombs (rich in metal alloys) were more volatile-rich than the scoriaceous bombs (poor in metal alloys), especially in sulfur. In fact, the sample that contained the most alloys (Strom1) was the richest in whole-rock sulfur, pre-eruptive sulfur (melt inclusions), and post-eruptive sulfur (matrix glass). The pumiceous bombs also contained more chlorine than the scoriaceous bombs, but the

difference was not as dramatic. This could indicate that sulfur is as important as chlorine, if not more important in the transport of the metals that make up the metal alloys.

Many researchers have studied the relative importance of sulfur versus chlorine in the transport of metals for hydrothermal ore deposits. It is widely acknowledged that metals are likely transported from the host magmas as metal-chloride complexes (Shinohara, 1994). Two of the major constituents of the metal alloys (Co and Sn) are likely transported in this manner by vapor-phase chlorides. However, the third component Cu does not always complex with Cl in the vapor phase very well. Nagaseki and Hayeshi (2004) studied the effect S has on the transport of metals. They performed laboratory tests on vapor and brine inclusions and found that inclusions without S contained no detectable Cu in the vapor. However, when sulfur was added, the vapor inclusions had thousands ppm of Cu. They realized that with the addition of sulfur, Cu preferentially fractionated into the vapor phase.

Simon et al. (2006) also studied the effect sulfur has on Cu partitioning between vapor and NaCl-rich brine. They found that without the addition of S, Cu preferentially partitioned into the high-salinity brine. However, when S was added, the mass transfer of Cu to the vapor phase significantly increased. They believe this is because of sulfur ligands that complex with the Cu. Heinrich et al. (1999) proposed that HS^- is a likely candidate for this ligand.

5.4 Formation of the metal alloys

The sulfur maps are snapshots of the results of variable degassing of sulfur as it moved to the vesicles. There are two possible interpretations for what these variable degassing patterns indicate. They could be showing that sulfur is using micro-fractures in

glass or melt (perhaps caused by shearing) as paths to the vesicle. This process is seen on a larger scale in rhyolite lava flows, where volatiles flow along shear planes in deforming lava. Vapor-phase minerals such as quartz, feldspar, Fe-oxides and topaz crystallize along these flow foliations.

Another process that might cause these patterns, however, is the deformation of small vesicles around inflating vesicles. Perhaps the dark, S-poor bands are the remnants of these vesicles that were deformed by larger inflating vesicles.

We speculate that, as sulfur and chlorine degass in the cooling bombs and move through the glass along small-scale flow paths, they complex with dissolved metals and carry them to the inflating vesicles (Fig. 15). Because the interior of the bombs cool more slowly, and become crystalline, more volatiles are exsolved and expelled to the vesicles and more metal alloys form after reduction of the metals. Moving outward toward the quenched, glassy rind of the bomb, the number of alloy grains decreases as the amount of trapped volatiles in the vesicles decreases.

Once the vapor-phase metal sulfides and chlorides reach the inflated vesicles, they cool and condense as they are reduced, forming the metal alloys (Fig. 16). H_2 gas could produce this reducing environment, and it is a common, although small, component of volcanic vapors. Reactions that could form the native metals that make up the metal alloy grains include, but are not limited to, the following:

$2AuHS + H_2 = 2H_2S + 2Au^o$

$2CuCl + H_2 = 2HCl + 2Cu^o$

$CoCl_2 + H_2 = 2HCl + Co^o$

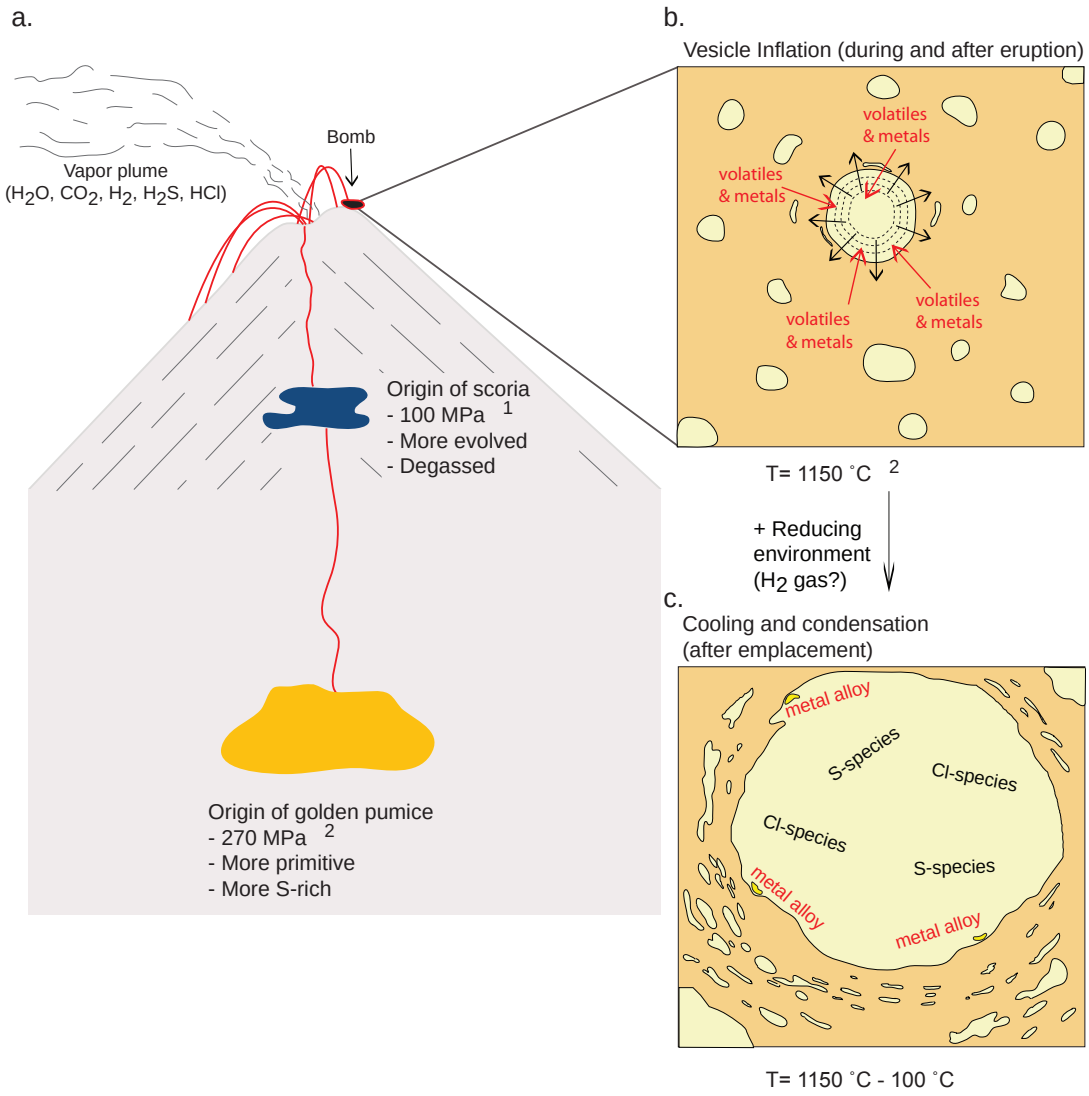

Figure 16. Model of the processes at Stromboli that may be involved in the formation of the metal alloy grains. a. The pumiceous bombs rich in metal alloys likely originated from a deeper magma that was more primitive and volatile-rich. The scoriaceous bombs (alloy-poor) originated from a more shallow magma that was relatively degassed. b. When they bombs were erupted, volatiles and the metals they complex with (metal-rich sulfides and chlorides) moved towards inflating vesicles. c. During cooling and condensation, the metals were reduced (perhaps by the addition of the H2 gas) to form the metal alloy grains.

[1] Pressure of scoria magma from Metrich et al., 2001
[2] Pressure of golden pumice magma and temperature from Di Carlo et al., 2006

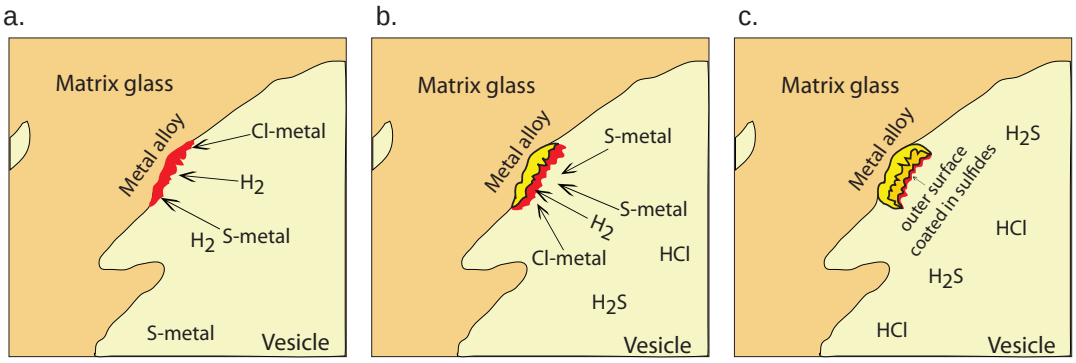

Figure 17. Model of how metal alloy grains form and grow. a. During cooling and condensation, metal-rich sulfides and chlorides are reduced on the vesicle wall, perhaps by the addition of H_2 gas, and condense onto the walls of vesicles. b. As the reduced metals condense onto the vesicle walls, H_2S and HCl (products of the reducing reactions) fill the vesicle. c. Eventually, the reducing environment in the vesicle disappears. The excess metal-rich sulfides (and chlorides) condense onto the outer surface of the metal alloys.

The reduced metals are deposited on the curved edge of the vesicle, and as the reducing process continues, the metal alloy grains grow out into the interior of the vesicles, forming a cockscomb growth structure. Eventually, the reducing environment disappears and only metal sulfides and possibly chlorides are deposited on the outer surfaces of the alloy grains. At the end of this process, H_2S and HCl are free to escape from the vesicles through fractures as the bombs cool.

6. Conclusion

Volatile phase transport and deposition of metals either as chlorides/sulfides or as metal alloys appears to be a common process. The pumiceous bombs collected are more primitive and S-rich and thus contain more metal alloy grains of a larger size than the more-evolved, degassed scoriaceous bombs. The conditions that the metal alloys form under are likely varied but there are several factors that seem to be especially important in their formation. Cooling history between the slowly-cooled interior and the glassy rind affects the number of alloys, reflecting the importance of trapped volatiles in the vesicles. The amount of volatiles also affects the number and size of the alloys. Non-degassed primitive magma may provide more complexing and transporting volatiles (but not necessarily more metals) to create the higher abundance of alloys hosted by the vesicles. Sulfur is especially vital and perhaps reflects the importance of this element in larger scale ore deposits.

7. References

Allard, P., Aiuppa, A., Loyer, H., Carrot, F., Gaudry, A., Pinte, G., Michel, A., and Dongarra, G., 2000. Acid gas and metal emission rates during long-lived basalt degassing at Stromboli volcano. Geophysical Research Letters, 27: 1207-1210.

Allard, P., Carbonelle, J., Metrich, N., Loyer, H., and Zettwoog, P., 1994. Sulphur output and magma degassing of Stromboli volcano. Nature, 368: 326-330.

Baker, D.R., Freda, C., Brooker, R.A., and Scarlato, P., 2008. The fidelity of melt inclusions as records of melt composition. Contributions to Mineralogy and Petrology, 156: 377-395

Bertagnini, A., Metrich, N., Landi, P., and Rosi, M., 2003. Stromboli volcano (Aeolian Archipelago, Italy): An open window on the deep-feeding system of a steady state basaltic volcano. Journal of Geophysical Research, 108: 4-1- 4-15.

Cortes, J.A., Wilson, M., Condliffe, E., and Francalanci, L., 2006. The ocurrence of forsterite and highly oxidizing conditions in basaltic lavas from Stromboli volcano, Italy. Journal of Petrology, 47: 1345-1373.

Cortes, J.A., Wilson, M., Condliffe, E., Francalanci, L., and Chertkoff, D.G., 2005. The evolution of the magmatic system of Stromboli volcano during the Vancori period (26-13.8 ky). Journal of Volcanology and Geothermal Research, 147: 1-38.

Danyushevsky, L.V., McNeill, A.W., and Sobolev, A.V., 2002. Experimental and petrological studies of melt inclusions in phenocrysts of melt inclusions in phenocrysts from mantle-derived magmas: an overview of techniques, advantages and complications. Chemical Geology, 183: 5-24.

Di Carlo, I., Pichavant, M., Rotolo, S.G., Scaillet, B., 2006. Experimental crystallization of a high-K arc basalt: the Golden Pumice, Stromboli Volcano (Italy). Journal of Petrology, 47: 1317-1343.

Francalanci, L., Davies, G.R., Lustenhower, W., Tommasini, S., Mason, P.R.D., and Conticelli, S., 2005. Intra-grain Sr istope evidence for crystal recycling and multiple magma reservoirs in the recent activity of Stromboli Volcano, Southern Italy. Journal of Petrology, 46: 1997-2016.

Francalanci, L., Tommasini, S., and Conticelli, S., 2004. The volcanic activity of Stromboli in the 1906-1998 AD period: mineralogical, geochemical and isotope data relevant to the understanding of the plumbing system. Journal of Volcanology and Geothermal Research, 131: 179-211.

Francalanci, L., Manetti, P., and Peccerillo, A., Keller, J., 1993. Magmatological evolution of the Stromboli Volcano (Aeolian Arc, Italy): Inferences from major and trace

element and Sr isotopic composition of lavas and pyroclastic rocks. Acta Vulcanologica, 3: 127-151.

Francalanci, L., Manetti, P., and Peccerillo, A., 1989. Volcanological and magmatological evolution of Stromboli volcano (Aeolian Islands): the roles of fractional crystallization, magma mixing, crustal contamination and source heterogeneity. Bulletin of Volcanology, 51: 355-378.

Gvirtzman, Z. and Nur, A., 1999. The formation of Mount Etna as the consequence of slab rollback. Nature, 401: 782-785.

Heinrich, C.A., Günther, D., Audétat, A., Ulrich, T., and Frischknecht, R., 1999. Metal fractionation between magmatic brine and vapor, determined by microanalysis of fluid inclusions. Geology, 27: 755-758.

Hunter, B., 2007. The smallest base and precious metal deposits in the world: Vapor transport and deposition of bronze-Co-Ag alloys in vesicles. M.S. Thesis, Brigham Young University, Provo, Utah.

Keller, G., 2001. Applied statistics with Microsoft® Excel. Duxbury Thomson Learning, CA.

Keller, J., Hornig-Kjarsgaard, I., Koberski, U., Stadlbauer, E., and Lenhard, R., 1993. Geological Map of Stromboli 1:10000. Acta Vulcanologia, 3: 21-68.

Laiolo, M., and Cigolini, C., 2006. Mafic and ultramafic xenoliths in San Bartolo lava field: New insights on the ascent and storage of Stromboli magmas. Bulletin of Volcanology, 68: 653-670.

Landi, P., Francalanci, L., Pompilio, M., Rosi, M., Corsaro, R., Petrone, C., Nardini, I., and Miraglia, L., 2006. The December 2002-July 2003 effusive event at Stromboli volcano, Italy: Insights into the shallow plumbing system by petrochemical studies. Journal of Volcanology and Geothermal Research, 155: 263-284.

Landi, P., Metrich, N., Bertagnini, A., and Rosi, M., 2004. Dynamics of magma mixing and degassing recorded in plagioclase at Stromboli (Aeolian Archipelago, Italy). Contributions to Mineralogy and Petrology, 147: 213-227.

Larocque, A., Stimac, J., Siebe, C., Greengrass, K., Chapman, R., and Mejia, S., 2008. Deposition of a high-sulfidation Au assemblage from a magmatic volatile phase, Volcán Popocatépetl, Mexico. Journal of Volcanology and Geothermal Research. 170: 51-60.

Liu, Y., Samaha, N., Baker, D.R., 2007. Sulfur concentration at sulfide saturation (SCSS) in magmatic silicate melts. Geochimica et Cosmochimica Acta, 71: 1783-1799.

Luhr, J., 2001. Glass inclusions and melt volatile content at Parícutin Volcano, Mexico. Contributions to Mineralogy and Petrology, 142: 261-283.

McDonough, W.F., and Sun, S., 1989. The composition of the Earth. Chemical Geology, 120: 223-253.

Metrich, N., Bertagnini, A., Landi, P., and Rosi, M., 2001. Crystallization driven by decompression and water loss at Stromboli Volcano (Aeolian Islands, Italy). Journal of Petrology, 42: 1471-1490.

Nagaseki, H., and Hayashi K., 2004. Vapor-liquid partitioning experiment of ore metals in boiling hydrothermal solutions using synthetic fluid inclusions [abs]: Society of Resource Geology Annual Meeting, Tokyo, June, 2004, Abstracts, p. 17 (in Japanese).

Ripepe, M., Marchetti, E., Ulivieri, G., Harris, A., Dehn, J., Burton, M., Caltabiano, T., and Salerno, G., 2005. Effusive to explosive transition during the 2003 eruption of Stromboli volcano. Geology, 33: 341-344.

Rosi, M., Bertagnini, A., and Landi, P., 2000. Onset of the persistent activity at Stromboli volcano (Italy). Bulletin of Volcanology, 62: 294-300.

Shinohara, H., 1994. Exsolution of immiscible vapor and liquid phases from a crystallizing silicate melt: Implications for chlorine and metal transport. Geochimica et Cosmochimica Acta, 58: 5215-5221.

Simon, A., Pettke, T., Candela, P., Piccoli, P., Heinrich, C., 2006. Copper partitioning in a melt-vapor-brine-magnetite-pyrrhotite assemblage. Geochimica et Cosmochimica Acta, 70: 5583-5600.

Strand, S.R., Keith, J.D., Dorais, M.J., Stavast, W.J.A., Aase, J., Harper, M.P., Harris, W.B., Syme, A.K., Henderson, R., Porter, J., Ashley, S.E., 2002. Mobility of copper, chlorine, and sulfur during quenching of Hawaiian basaltic magmas. Abstract with Programs,Geological Society of America, 34: 88.

Williams-Jones, A., and Heinrich, C., 2005. Vapor transport of metals and the formation of magmatic-hydrothermal ore deposits. Economic Geology, 100: 1287-1312.

8. Appendices

8.1 Sample descriptions

Strom07-1: Scoriaceous bomb

Hand sample size (long dimension x height): 180 mm x 55 mm

Hand sample description: Grey to black scoriaceous bomb with glassy rind that, in some areas, has a silver sheen. Moving towards the center, sample becomes increasingly vesicular and contains larger phenocrysts. Plagioclase is the most visible phenocryst.

Phenocryst modal percentage: 20% vesicles, 25% fine-grained groundmass/glass, 25% plagioclase, 20% clinopyroxene, 10% olivine

Olivine: Fo_{72-74}

Clinopyroxene: Wo_{42-44} Fer_{9-16}

Plagioclase: An_{62-86}

Strom07-2: Scoriaceous bomb

Hand sample size (long dimension x height): 85 mm x 25 mm

Hand sample description: Grey to black scoriaceous bomb with glassy rind that, in some areas, has a silver sheen. Moving towards the center, sample becomes increasingly vesicular and contains larger phenocrysts. Plagioclase and olivine are the most visible phenocrysts.

Phenocryst modal percentage: 15% vesicles, 40% fine-grained groundmass/glass, 30% plagioclase, 10% clinopyroxene, 5% olivine

Olivine: Fo_{72-73}

Clinopyroxene: Wo_{42-44} Fer_{12-15}

Strom07-5: Scoriaceous bomb

Hand sample size (long dimension x height): 140 mm x 50 mm

Hand sample description: Grey to black scoriaceous bomb with glassy rind that, in some areas, has a silver sheen. Moving towards the center, sample becomes increasingly vesicular and contains larger phenocrysts. Plagioclase is the most visible phenocryst.

Olivine: Fo_{71-73}

Clinopyroxene: Wo_{40-44} Fer_{12-15}

Strom1: Pumiceous bomb

Hand sample size (long dimension x height): 155 mm x 110 mm (broken)

Hand sample description: Dark yellow-brown pumiceous bomb with glassy rind. Sample has a flattened, ‘cow-pie’ morphology. Moving towards the center, sample becomes increasingly vesicular. Plagioclase is the most visible phenocryst.

Phenocryst modal percentage: 40% vesicles, 50% fine-grained groundmass/glass, 4% plagioclase, 5% clinopyroxene, 1% olivine

Olivine: Fo_{68-88}

Clinopyroxene: Wo_{38-47} Fer_{7-18}

Plagioclase: An_{61-90}

Strom5: Pumiceous bomb

Hand sample size (long dimension x height): 80x85 mm (broken)

Hand sample description: Dark yellow-brown pumiceous bomb with glassy rind. Sample has a flattened, ‘cow-pie’ morphology.Moving towards the center, sample becomes increasingly vesicular. Plagioclase is the most visible phenocryst.

Phenocryst modal percentage: 45% vesicles, 40% fine-grained groundmass/glass, 7% plagioclase, 6% clinopyroxene, 1% olivine

Olivine: Fo_{67-81}

Clinopyroxene: Wo_{39-45} Fer_{7-17}

8.2 Technique for separating olivine grains suitable for melt inclusion analysis

A fist-sized sample of each rock was crushed using a roller crusher. Then the powders were run through a magnetic separator to separate glass from minerals. Roll speed and vibrator were set to 24 and the magnet coil was set to 0.76 for all samples except Strom5. For Strom5 the magnet coil was set to 0.69. The separated minerals were then put through heavy liquids to separate the plagioclase (floats to the top) from the olivine and clinopyroxene (sinks to the bottom). The separated olivine and clinopyroxene were then examined under an optical microscope. The smaller dark green and brown green clinopyroxene and olivine fragments were handpicked and separated from the larger black clinopyroxene. The separated clinopyroxene and olivine fragments were then immersed in index oils and the melt inclusions were examined under plane-polarized light. Any fragments that had obvious fractures running through the melt inclusions were removed. The olivine and clinopyroxene fragments were then mounted with epoxy in one-inch round mounts and polished for electron microprobe analysis.

Appendix 8.3. Whole rock analyses of trace elements

Method			Strom1	Strom5	Strom 07-1	Strom 07-2	Strom 07-5
Fire assay	Au	ppm	0.005	0.003	0.003	0.002	0.001
fusion	Pt	ppm	<0.005	0.005	<0.005	0.005	0.006
and	Pd	ppm	0.009	0.008	0.005	0.006	0.005
ICP-AES							
Sulfur by	S	%	0.07	0.05	0.02	0.01	<0.01
Leco furnace							
4 acid 'near	Ag	ppm	0.13	0.11	0.18	0.13	0.15
near total'	Al	%	7.83	8.21	9.17	9.06	8.93
digestion	As	ppm	5.6	5.4	7.2	5.7	7.8
ICP-MS and	Ba	ppm	880	760	890	870	890
ICP-AES	Be	ppm	1.81	1.39	1.91	1.68	1.94
	Bi	ppm	0.12	0.16	0.33	0.16	0.12
	Ca	%	7.52	7.88	7.3	7.22	7.36
	Cd	ppm	0.09	0.09	0.08	0.08	0.07
	Ce	ppm	75	65	83	79.7	92.3
	Co	ppm	31.1	33.6	31.6	28.6	32.3
	Cr	ppm	87	23	71	71	72
	Cs	ppm	4.43	3.16	3.69	3.87	4.93
	Cu	ppm	99.4	110.5	111.5	93.3	93.8
	Fe	%	5.37	5.78	5.61	5.4	5.51
	Ga	ppm	16.65	17.7	16.55	15.5	17.5
	Ge	ppm	0.22	0.2	0.24	0.25	0.29
	Hf	ppm	3.8	3.5	4.2	4	4.3
	Hg	ppm	<0.01	<0.01	<0.01	<0.01	<0.01
	In	ppm	0.058	0.067	0.052	0.049	0.052
	K	%	1.8	1.51	1.65	1.64	1.68
	La	ppm	37.6	31.4	41.2	39.7	46.9
	Li	ppm	9.3	8.4	9.6	8.8	9.7
	Mg	%	3.55	3.52	3.59	3.47	3.56
	Mn	ppm	1035	1090	1090	1060	1095
	Mo	ppm	1.67	1.19	1.58	1.42	1.58
	Na	%	1.85	1.79	1.79	1.77	1.8
	Nb	ppm	22.5	18.1	20.5	18.6	21
	Ni	ppm	49.4	38.4	52.2	39.2	43.8
	P	ppm	2010	2290	2150	2070	2130
	Pb	ppm	18.6	14.6	18.6	17	18
	Rb	ppm	39.5	28.3	44.7	43.8	61.6
	Re	ppm	0.002	0.008	<0.002	<0.002	<0.002
	S	%	0.04	0.02	0.02	0.01	0.01
	Sb	ppm	0.48	0.27	0.5	0.25	0.26
	Sc	ppm	27.9	29	31.3	29.6	34.7

Appendix 8.3. cont.

Method			Strom1	Strom5	Strom 07-1	Strom 07-2	Strom 07-5
4 acid 'near	Se	ppm	1	1	2	2	2
near total'	Sn	ppm	1.8	1.6	1.7	1.5	1.7
digestion	Sr	ppm	760	764	735	726	734
ICP-MS and	Ta	ppm	1.08	0.94	1.1	1.06	1.13
ICP-AES	Te	ppm	<0.05	<0.05	<0.05	<0.05	<0.05
	Th	ppm	11.4	8.6	14.3	13.5	15.7
	Ti	%	0.459	0.519	0.49	0.485	0.502
	Tl	ppm	0.22	0.22	0.09	0.07	0.09
	U	ppm	4.1	3	4	3.6	4.1
	V	ppm	232	253	243	239	250
	W	ppm	2.3	1.6	2.2	1.9	2.1
	Y	ppm	21.3	21.5	24	22.5	26
	Zn	ppm	64	66	68	66	68
	Zr	ppm	157.5	143.5	156	143.5	158

Appendix 8.4. Olivine analyses from pumiceous and scoriaceous bombs

Pumiceous bombs

	strom1olv1	strom1olv1	strom1olv2	strom1olv2	strom1olv3
	core	rim	core	rim	core
SiO_2	37.82	37.99	37.81	37.90	39.93
TiO_2	0.02	0.01	0.01	0.02	0.02
Al_2O_3	0.05	0.01	0.02	0.04	0.02
FeO	24.81	24.58	25.07	25.30	15.51
MnO	0.47	0.49	0.47	0.47	0.27
NiO	0.06	0.11	0.03	0.02	0.18
MgO	36.28	36.23	36.45	36.20	44.00
CaO	0.34	0.36	0.33	0.32	0.28
Total	99.85	99.79	100.19	100.27	100.19
Fo	72.24	72.40	72.13	71.79	83.56
Mg#	0.72	0.72	0.72	0.72	0.83

	strom1olv3	strom1olv4	strom1olv4	strom1olv5	strom1olv5
	rim	core	rim	core	rim
SiO_2	40.38	37.01	40.84	37.10	39.19
TiO_2	0.00	0.02	0.01	0.02	0.04
Al_2O_3	0.05	0.02	0.03	0.05	0.04
FeO	15.58	29.54	11.91	28.18	18.05
MnO	0.26	0.58	0.22	0.54	0.31
NiO	0.13	0.00	0.19	0.04	0.06
MgO	44.03	33.00	47.17	33.83	42.19
CaO	0.31	0.24	0.27	0.24	0.29
Total	100.74	100.41	100.63	100.00	100.17
Fo	83.57	66.36	87.71	67.96	80.69
Mg#	0.83	0.67	0.88	0.68	0.81

	strom1olv6	strom1olv6	strom1olv7	strom1olv7	strom1-olv10
	core	rim	core	edge	core
SiO_2	37.12	39.82	38.89	39.57	38.64
TiO_2	0.02	0.01	0.00	0.02	0.00
Al_2O_3	0.04	0.03	0.06	0.04	0.08
FeO	26.27	16.63	20.00	17.06	20.10
MnO	0.47	0.29	0.38	0.30	0.37
NiO	0.07	0.09	0.07	0.12	0.11
MgO	34.98	43.05	40.67	42.90	39.57
CaO	0.24	0.26	0.33	0.31	0.34
Total	99.19	100.18	100.40	100.33	99.21
Fo	70.22	82.23	78.41	81.84	77.87
Mg#	0.70	0.82	0.78	0.82	0.78

Appendix 8.4 cont.

Pumiceous bombs

	strom1-olv10	strom1-olv11	strom1-olv11	strom1-olv11	strom1-olv11
	core	core	core	core	core
SiO_2	38.61	39.20	39.31	38.91	39.07
TiO_2	0.00	0.01	0.01	0.00	0.02
Al_2O_3	0.03	0.02	0.05	0.05	0.04
FeO	20.77	16.55	16.04	16.57	15.92
MnO	0.39	0.29	0.26	0.27	0.25
NiO	0.10	0.07	0.08	0.10	0.13
MgO	39.64	43.40	43.74	43.26	43.60
CaO	0.33	0.28	0.28	0.27	0.30
Total	99.88	99.82	99.77	99.43	99.32
Fo	77.30	82.43	83.02	82.38	83.12
Mg#	0.77	0.82	0.83	0.82	0.83

	strom1-olv11	strom1b-olv1	strom1b-olv1	strom1b-olv1	strom1b-olv1
	core	core	core	core	rim
SiO_2	39.60	39.14	39.01	37.78	38.86
TiO_2	0.01	0.02	0.01	0.00	0.02
Al_2O_3	0.05	0.01	0.02	0.03	0.04
FeO	16.21	17.63	18.86	25.18	16.49
MnO	0.28	0.30	0.31	0.46	0.26
NiO	0.22	0.05	0.05	0.03	0.15
MgO	42.82	42.81	41.63	36.04	43.15
CaO	0.25	0.27	0.26	0.26	0.25
Total	99.42	100.22	100.15	99.78	99.22
Fo	82.52	81.27	79.75	71.74	82.40
Mg#	0.82	0.81	0.80	0.72	0.82

	strom1olv12	strom1olv12	strom5a-olv1	strom5a-olv1	strom5a-olv2
	core	rim	core	rim	core
SiO_2	38.08	37.45	37.27	36.92	37.07
TiO_2	0.02	0.02	0.02	0.02	0.01
Al_2O_3	0.05	0.03	0.05	0.03	0.01
FeO	16.84	27.14	26.47	26.07	26.22
MnO	0.29	0.48	0.51	0.49	0.49
NiO	0.11	0.03	0.06	0.02	0.05
MgO	43.50	33.69	36.03	36.54	36.03
CaO	0.25	0.22	0.36	0.35	0.34
Total	99.13	99.05	100.75	100.42	100.22
Fo	82.17	68.72	70.77	71.39	70.96
Mg#	0.82	0.69	0.71	0.71	0.71

Appendix 8.4 cont.

Pumiceous bombs

	strom5a-olv2	strom5a-olv3	strom5a-olv3	strom5aolv5	strom5aolv6
	rim	core	rim	core	core
SiO_2	37.15	36.70	36.53	39.77	37.83
TiO_2	0.02	0.02	0.02	0.01	0.01
Al_2O_3	0.03	0.02	0.02	0.03	0.04
FeO	25.58	26.37	25.82	18.71	26.85
MnO	0.46	0.50	0.48	0.33	0.51
NiO	0.07	0.00	0.02	0.05	0.04
MgO	36.19	35.31	36.35	41.21	34.91
CaO	0.36	0.35	0.38	0.33	0.36
Total	99.85	99.26	99.62	100.45	100.54
Fo	71.60	70.44	71.51	79.77	69.81
Mg#	0.72	0.70	0.72	0.80	0.70

	strom5aolv6	strom5aolv7	strom5aolv7	strom5aolv8	strom5aolv8
	rim	core	rim	core	rim
SiO_2	37.77	37.15	37.77	37.74	38.22
TiO_2	0.00	0.03	0.03	0.03	0.02
Al_2O_3	0.09	0.08	0.07	0.03	0.04
FeO	24.40	26.36	25.02	26.54	25.68
MnO	0.46	0.49	0.47	0.49	0.48
NiO	0.09	0.04	0.04	0.03	0.07
MgO	36.77	35.30	35.78	35.10	34.98
CaO	0.37	0.36	0.35	0.35	0.35
Total	99.95	99.79	99.52	100.29	99.84
Fo	72.88	70.45	71.80	70.18	70.79
Mg#	0.73	0.70	0.72	0.70	0.71

	stropm5bolv1	strom5bolv1	strom5bolv2	strom5bolv3	strom5bolv3
	core	rim	inclusion	core	core
SiO_2	37.24	37.25	36.35	37.43	36.85
TiO_2	0.02	0.03	0.02	0.02	0.01
Al_2O_3	0.03	0.04	0.02	0.02	0.06
FeO	26.83	25.94	29.26	26.30	25.90
MnO	0.49	0.51	0.56	0.50	0.49
NiO	0.02	0.04	0.04	0.00	0.06
MgO	35.64	36.42	33.48	35.20	35.90
CaO	0.34	0.34	0.25	0.34	0.36
Total	100.62	100.57	99.97	99.80	99.62
Fo	70.26	71.39	66.93	70.42	71.16
Mg#	0.70	0.71	0.67	0.70	0.71

Appendix 8.4 cont.

Pumiceous bombs

	strom5bolv3	strom5bolv1	strom5bolv1	strom5bolv4	strom5bolv4
	rim	core	rim	core	rim
SiO_2	37.35	37.45	39.59	37.44	37.81
TiO_2	0.01	0.03	0.01	0.01	0.02
Al_2O_3	0.04	0.04	0.04	0.08	0.06
FeO	25.48	28.35	18.50	26.59	25.83
MnO	0.46	0.50	0.32	0.47	0.47
NiO	0.05	0.00	0.07	0.09	0.06
MgO	35.64	33.43	41.44	35.22	35.83
CaO	0.36	0.29	0.29	0.36	0.37
Total	99.38	100.09	100.26	100.26	100.43
Fo	71.37	67.66	80.01	70.24	71.20
Mg#	0.71	0.68	0.80	0.70	0.71

	strom5bolv6	strom5bolv6	strom5b-olv7	strom5olv10	strom5olv10
	core	rim	core	core	rim
SiO_2	37.90	37.76	37.02	37.57	38.63
TiO_2	0.01	0.02	0.02	0.01	0.01
Al_2O_3	0.05	0.09	0.03	0.05	0.04
FeO	25.71	25.27	26.89	28.12	20.89
MnO	0.48	0.47	0.47	0.50	0.36
NiO	0.04	0.13	0.04	0.08	0.05
MgO	35.75	35.58	35.50	33.38	39.50
CaO	0.36	0.38	0.33	0.31	0.29
Total	100.30	99.69	100.30	100.03	99.77
Fo	71.23	71.52	70.13	67.83	77.13
Mg#	0.71	0.71	0.70	0.68	0.77

	strom5olv11	strom5olv11	strom5olv12
	core	rim	core
SiO_2	38.77	38.79	36.70
TiO_2	0.00	0.00	0.02
Al_2O_3	0.00	0.05	0.03
FeO	19.88	17.90	26.84
MnO	0.33	0.32	0.52
NiO	0.02	0.07	0.04
MgO	40.77	43.00	35.08
CaO	0.27	0.27	0.32
Total	100.03	100.39	99.55
Fo	78.54	81.09	69.88
Mg#	0.79	0.81	0.70

Appendix 8.4 cont.

Scoriaceous bombs

	strom07-1olv2	strom07-1olv2	strom07-1olv1	strom07-1olv1	strom07-1olv3
	core	rim	core	rim	core
SiO_2	38.38	38.26	37.56	37.97	37.75
TiO_2	0.00	0.02	0.00	0.02	0.02
Al_2O_3	0.04	0.04	0.02	0.01	0.04
FeO	23.44	24.18	24.67	24.27	24.92
MnO	0.42	0.45	0.46	0.46	0.46
NiO	0.11	0.00	0.04	0.04	0.06
MgO	37.08	36.65	36.39	36.57	36.30
CaO	0.37	0.36	0.32	0.32	0.34
Total	99.83	99.96	99.44	99.65	99.88
Fo	73.87	72.99	72.41	72.82	72.16
Mg#	0.74	0.73	0.72	0.73	0.72

	strom07-1olv3	strom07-1olv4	strom07-1olv4	strom07-1olv17	strom07-2olv4
	rim	core	rim	core	core
SiO_2	38.14	38.34	37.88	37.46	36.80
TiO_2	0.03	0.01	0.01	0.01	0.01
Al_2O_3	0.02	0.04	0.04	0.03	0.01
FeO	24.59	24.30	24.48	24.79	24.77
MnO	0.46	0.47	0.46	0.47	0.46
NiO	0.02	0.09	0.07	0.16	0.07
MgO	36.19	36.54	36.23	36.83	37.04
CaO	0.35	0.33	0.35	0.34	0.31
Total	99.81	100.12	99.52	100.08	99.46
Fo	72.39	72.79	72.50	72.55	72.66
Mg#	0.72	0.73	0.73	0.73	0.73

	strom07-2olv4	strom07-2olv5	strom07-2olv5	strom07-2olv6	strom07-2olv2
	rim	core	rim	core	core
SiO_2	37.18	37.17	37.13	37.03	36.72
TiO_2	0.03	0.01	0.01	0.02	0.00
Al_2O_3	0.02	0.01	0.01	0.02	0.03
FeO	24.33	24.88	24.56	24.65	24.34
MnO	0.47	0.45	0.50	0.47	0.49
NiO	0.03	0.07	0.03	0.07	0.10
MgO	36.74	36.99	37.05	36.52	37.01
CaO	0.35	0.32	0.36	0.31	0.34
Total	99.14	99.89	99.65	99.08	99.02
Fo	72.90	72.56	72.85	72.47	73.00
Mg#	0.73	0.73	0.73	0.73	0.73

Appendix 8.4 cont.

Scoriaceous bombs

	strom07-2olv2	strom07-2olv3	strom07-5olv2	strom07-5olv2	strom07-5olv1
	rim	core	core	rim	core
SiO_2	36.78	36.61	37.37	37.36	37.04
TiO_2	0.00	0.03	0.01	0.02	0.01
Al_2O_3	0.03	0.05	0.03	0.04	0.02
FeO	24.75	24.37	24.16	24.35	24.64
MnO	0.46	0.48	0.46	0.44	0.48
NiO	0.03	0.05	0.05	0.11	0.12
MgO	36.97	37.21	36.75	36.70	36.86
CaO	0.34	0.32	0.31	0.32	0.32
Total	99.36	99.10	99.13	99.33	99.49
Fo	72.67	73.08	73.01	72.85	72.66
Mg#	0.73	0.73	0.73	0.73	0.73

	strom07-5olv1	strom07-5olv3	strom07-5olv15	strom07-5olv15	strom07-5olv16
	rim	core	core	core	core
SiO_2	37.12	37.15	37.22	37.60	37.75
TiO_2	0.02	0.03	0.03	0.01	0.01
Al_2O_3	0.04	0.03	0.05	0.02	0.03
FeO	24.16	24.84	25.05	24.80	25.40
MnO	0.45	0.47	0.47	0.47	0.48
NiO	0.04	0.04	0.00	0.01	0.06
MgO	36.98	37.06	35.97	35.99	35.78
CaO	0.35	0.30	0.34	0.33	0.32
Total	99.16	99.92	99.14	99.23	99.83
Fo	73.16	72.61	71.88	72.08	71.45
Mg#	0.73	0.73	0.72	0.72	0.72

	strom07-5olv17	strom07-5olv4	strom07-5olv4
	core	core	rim
SiO_2	37.69	38.48	38.83
TiO_2	0.00	0.02	0.02
Al_2O_3	0.03	0.03	0.03
FeO	24.75	24.46	24.46
MnO	0.46	0.45	0.46
NiO	0.05	0.03	0.04
MgO	36.64	35.92	36.14
CaO	0.33	0.32	0.36
Total	99.96	99.71	100.34
Fo	72.49	72.32	72.48
Mg#	0.73	0.72	0.72

Appendix 8.5. Analyses of clinopyroxene from pumiceous and scoriaceous bombs

Pumiceous bombs

	strom1cpx4	strom1cpx4	strom1cpx3	strom1cpx3
	core	rim	core	core
SiO_2	50.68	50.86	50.34	50.32
TiO_2	0.82	0.61	0.83	0.97
Al_2O_3	3.34	5.29	3.84	3.60
FeO	10.28	5.35	8.35	10.35
MnO	0.27	0.11	0.20	0.28
MgO	14.63	15.21	14.00	14.30
CaO	18.86	21.60	21.40	19.28
Na_2O	0.34	0.26	0.33	0.39
Total	99.23	99.29	99.29	99.49
En	0.43	0.45	0.41	0.42
Fer	0.17	0.09	0.14	0.17
Wo	0.40	0.46	0.45	0.41
Mg#	0.72	0.84	0.75	0.71

	strom1cpx5	strom1cpx5	strom1cpx1	strom1cpx1
	core	rim	core	rim
SiO_2	51.36	51.26	51.42	51.78
TiO_2	0.72	0.50	0.56	0.38
Al_2O_3	2.87	4.30	2.57	4.22
FeO	8.89	4.41	9.69	4.13
MnO	0.24	0.10	0.27	0.11
MgO	14.70	16.21	14.71	16.06
CaO	20.36	22.35	19.62	22.51
Na_2O	0.36	0.21	0.29	0.22
Total	99.50	99.32	99.12	99.42
En	0.43	0.47	0.43	0.46
Fer	0.15	0.07	0.16	0.07
Wo	0.43	0.46	0.41	0.47
Mg#	0.75	0.87	0.73	0.87

Appendix 8.5 cont.

Pumiceous bombs

	strom1cpx2	strom1cpx2	strom1cpx6	strom1cpx6
	core	rim	core	rim
SiO_2	50.72	52.33	50.71	52.91
TiO_2	0.80	0.35	0.76	0.34
Al_2O_3	3.12	2.90	2.97	2.71
FeO	10.77	4.45	11.20	4.51
MnO	0.32	0.12	0.31	0.12
MgO	14.82	16.68	14.79	16.71
CaO	18.44	22.37	17.96	22.16
Na_2O	0.32	0.24	0.33	0.20
Total	99.30	99.42	99.03	99.65
En	0.43	0.47	0.44	0.48
Fer	0.18	0.07	0.18	0.07
Wo	0.39	0.46	0.38	0.45
Mg#	0.71	0.87	0.70	0.87

	strom1cpx7	strom1cpx7	strom5bpyx4	strom5bpyx4
	core	rim	core	rim
SiO_2	49.53	51.40	51.40	52.58
TiO_2	0.87	0.55	0.54	0.37
Al_2O_3	4.72	4.68	2.76	2.86
FeO	8.93	4.69	8.21	4.59
MnO	0.20	0.11	0.29	0.10
MgO	13.34	15.85	14.92	16.80
CaO	21.09	22.22	20.73	22.16
Na_2O	0.35	0.26	0.22	0.11
Total	99.02	99.74	99.07	99.56
En	0.40	0.46	0.43	0.48
Fer	0.15	0.08	0.13	0.07
Wo	0.45	0.46	0.43	0.45
Mg#	0.73	0.86	0.76	0.87

Appendix 8.5 cont.

Pumiceous bombs

	strom5bcpx4	strom5bcpx4	strom5bpyx1	strom5bpyx1
	core	rim	core	edge
SiO_2	51.64	50.93	51.19	50.24
TiO_2	0.62	0.59	0.77	1.06
Al_2O_3	3.00	5.03	3.07	3.68
FeO	8.34	4.64	9.97	8.44
MnO	0.28	0.10	0.30	0.22
MgO	14.73	15.65	14.91	14.25
CaO	20.86	22.66	19.17	21.05
Na_2O	0.36	0.17	0.21	0.20
Total	99.83	99.77	99.60	99.14
En	0.43	0.45	0.44	0.42
Fer	0.14	0.08	0.16	0.14
Wo	0.44	0.47	0.40	0.44
Mg#	0.76	0.86	0.73	0.75

	strom5bcpx5	strom5bcpx5	strom5bcpx6	strom5bcpx7
	core	rim	core	core
SiO_2	51.67	51.71	51.05	50.62
TiO_2	0.45	0.76	0.78	0.92
Al_2O_3	3.43	2.70	3.03	3.48
FeO	6.49	7.85	10.45	8.08
MnO	0.18	0.23	0.34	0.18
MgO	15.22	15.03	14.84	14.63
CaO	21.70	20.93	18.55	21.22
Na_2O	0.27	0.31	0.33	0.30
Total	99.40	99.52	99.37	99.44
En	0.44	0.44	0.44	0.42
Fer	0.11	0.13	0.17	0.13
Wo	0.45	0.44	0.39	0.44
Mg#	0.81	0.77	0.72	0.76

Appendix 8.5 cont.

Pumiceous bombs

	strom5bcpx7
	rim
SiO_2	50.27
TiO_2	0.93
Al_2O_3	3.43
FeO	8.46
MnO	0.23
MgO	14.33
CaO	20.66
Na_2O	0.34
Total	98.66
En	0.42
Fer	0.14
Wo	0.44
Mg#	0.75

Scoriaceous bombs

	strom07-1cpx1	strom07-1cpx1	strom07-1cpx2	strom07-1cpx2
	core	rim	core	core
SiO_2	53.08	50.49	49.79	50.75
TiO_2	0.46	0.92	0.97	0.84
Al_2O_3	1.90	3.75	3.95	2.97
FeO	5.45	7.86	9.82	8.25
MnO	0.18	0.22	0.26	0.23
MgO	16.75	14.47	14.00	14.57
CaO	21.51	21.13	19.59	20.80
Na_2O	0.23	0.29	0.38	0.29
Total	99.55	99.12	98.75	98.70
En	0.47	0.42	0.42	0.43
Fer	0.09	0.13	0.16	0.14
Wo	0.44	0.45	0.42	0.44
Mg#	0.85	0.77	0.72	0.76

Appendix 8.5 cont.

Scoriaceous bombs

	strom07-1cpx2	strom07-1cpx3	strom07-1cpx3	strom07-1cpx4
	rim	core	rim	core
SiO_2	52.23	50.90	51.64	50.96
TiO_2	0.63	0.75	0.70	0.82
Al_2O_3	2.33	2.99	2.75	3.47
FeO	7.80	9.49	7.93	8.30
MnO	0.24	0.29	0.23	0.20
MgO	15.43	14.43	14.80	14.51
CaO	20.45	19.62	20.75	20.53
Na_2O	0.25	0.29	0.34	0.33
Total	99.35	98.76	99.14	99.11
En	0.45	0.43	0.43	0.43
Fer	0.13	0.16	0.13	0.14
Wo	0.43	0.42	0.44	0.43
Mg#	0.78	0.73	0.77	0.76

	strom07-1cpx4	strom07-2cpx1	strom07-2cpx2	strom07-2cpx3
	rim	core	rim	core
SiO_2	51.26	50.32	50.43	51.37
TiO_2	0.69	0.96	0.93	0.71
Al_2O_3	2.66	3.32	3.43	3.01
FeO	7.77	8.22	8.18	7.33
MnO	0.19	0.24	0.22	0.20
MgO	14.99	14.52	14.49	15.22
CaO	20.93	20.67	21.08	21.09
Na_2O	0.29	0.35	0.29	0.29
Total	98.78	98.61	99.05	99.21
En	0.44	0.43	0.42	0.44
Fer	0.13	0.14	0.13	0.12
Wo	0.44	0.44	0.44	0.44
Mg#	0.77	0.76	0.76	0.79

Appendix 8.5 cont.

Scoriaceous bombs

	strom07-2cpx3	strom07-2cpx4	strom07-2cpx4	strom07-2cpx5
	rim	core	rim	core
SiO_2	50.91	51.00	50.47	50.18
TiO_2	0.92	0.58	0.92	1.04
Al_2O_3	3.65	2.67	3.52	4.02
FeO	7.86	8.33	7.81	8.98
MnO	0.21	0.26	0.22	0.22
MgO	14.65	15.26	14.69	13.89
CaO	20.93	20.42	20.90	20.80
Na_2O	0.29	0.30	0.31	0.34
Total	99.42	98.81	98.83	99.46
En	0.43	0.44	0.43	0.41
Fer	0.13	0.14	0.13	0.15
Wo	0.44	0.42	0.44	0.44
Mg#	0.77	0.77	0.77	0.73

	strom07-2cpx5	strom07-2cpx6	strom07-2cpx6	strom07-5cpx3
	rim	core	rim	rim
SiO_2	50.50	52.10	50.80	50.25
TiO_2	0.93	0.69	0.73	0.89
Al_2O_3	3.65	2.59	2.85	3.55
FeO	7.86	9.06	7.63	7.61
MnO	0.21	0.27	0.21	0.19
MgO	14.77	15.25	15.14	14.76
CaO	21.08	19.72	20.91	20.99
Na_2O	0.31	0.32	0.29	0.29
Total	99.32	99.99	98.56	98.53
En	0.43	0.44	0.44	0.43
Fer	0.13	0.15	0.12	0.12
Wo	0.44	0.41	0.44	0.44
Mg#	0.77	0.75	0.78	0.78

Appendix 8.5 cont.

Scoriaceous bombs

	strom07-5cpx1c	strom07-5cpx1	strom07-5cpx2	strom07-5cpx2
	core	rim	core	rim
SiO_2	51.05	51.21	50.61	50.77
TiO_2	0.71	0.85	0.85	0.84
Al_2O_3	2.69	3.57	3.68	3.27
FeO	9.33	7.60	9.18	7.64
MnO	0.32	0.18	0.26	0.20
MgO	15.04	14.75	14.16	14.89
CaO	19.11	21.05	19.87	21.14
Na_2O	0.40	0.28	0.35	0.27
Total	98.64	99.50	98.97	99.02
En	0.44	0.43	0.42	0.43
Fer	0.15	0.12	0.15	0.12
Wo	0.40	0.44	0.42	0.44
Mg#	0.74	0.78	0.73	0.78

	strom07-5cpx5
	rim
SiO_2	51.60
TiO_2	0.90
Al_2O_3	3.55
FeO	7.47
MnO	0.21
MgO	14.81
CaO	21.06
Na_2O	0.27
Total	99.87
En	0.43
Fer	0.12
Wo	0.44
Mg#	0.78

Appendix 8.6. Plagioclase analyses for pumiceous (Strom1) and scoriaceous (Strom07-1) bombs

Pumiceous bombs

	strom1plag1	strom1plag2	strom1plag3	strom1plag3	strom1plag4
	rim	core	core	rim	core
SiO_2	52.49	45.47	47.07	46.21	46.07
Al_2O_3	29.54	33.07	34.04	33.45	34.73
Fe_2O_3	0.72	1.30	0.43	0.58	0.55
CaO	12.62	17.53	17.64	16.98	18.19
Na_2O	3.96	1.32	1.59	1.66	1.10
K_2O	0.79	0.28	0.16	0.18	0.08
Total	100.12	98.97	100.92	99.06	100.71
Ab	0.35	0.12	0.14	0.15	0.10
An	0.61	0.87	0.85	0.84	0.90
Or	0.05	0.02	0.01	0.01	0.00

	strom1plag4	strom1plag5	strom1plag5
	rim	core	rim
SiO_2	45.99	45.74	46.00
Al_2O_3	34.52	34.49	34.23
Fe_2O_3	0.58	0.56	0.58
CaO	18.12	17.94	17.64
Na_2O	1.18	1.27	1.37
K_2O	0.08	0.10	0.15
Total	100.48	100.10	99.97
Ab	0.10	0.11	0.12
An	0.89	0.88	0.87
Or	0.00	0.01	0.01

Scoriaceous bombs

	strom07-1plag1	strom07-1plag1	strom07-1plag2	strom07-1plag2	strom07-1plag3
	core	rim	core	rim	rim
SiO_2	52.13	47.02	47.29	48.79	47.20
Al_2O_3	29.99	33.41	32.99	31.10	33.72
Fe_2O_3	0.69	0.94	0.84	0.98	0.80
CaO	12.82	17.04	16.89	14.57	17.18
Na_2O	3.85	1.75	1.85	2.86	1.49
K_2O	0.74	0.23	0.22	0.49	0.16
Total	100.21	100.38	100.09	98.80	100.55
Ab	0.34	0.15	0.16	0.25	0.13
An	0.62	0.83	0.82	0.72	0.86
Or	0.04	0.01	0.01	0.03	0.01

Appendix 8.6 cont.

Scoriaceous bombs

	strom07-1plag4	strom07-1plag4	strom07-1plag5	strom07-1plag5
	core	rim	core	rim
SiO_2	47.74	51.10	46.51	50.38
Al_2O_3	32.37	30.59	33.70	31.21
Fe_2O_3	0.84	0.68	0.79	0.93
CaO	15.83	13.61	17.40	14.47
Na_2O	2.34	3.43	1.56	3.09
K_2O	0.34	0.59	0.18	0.49
Total	99.47	100.00	100.14	100.55
Ab	0.21	0.30	0.14	0.27
An	0.77	0.66	0.85	0.70
Or	0.02	0.03	0.01	0.03

Appendix 8.7. Olivine melt inclusions from pumiceous and scoriaceous bombs

Pumiceous bombs

	strom1 olv7m1	strom1 olv7m2	strom1 olv11m1	strom1 olv11m2	strom1 olv11m3	strom1 olv1m1	strom1 olv1m3
SiO_2	51.06	50.70	50.92	52.29	50.55	50.78	51.04
TiO_2	0.92	0.94	0.92	0.89	0.90	1.01	1.02
Al_2O_3	17.45	17.43	17.97	17.97	18.38	18.84	17.82
FeO_{total}	7.97	8.14	7.33	7.04	7.60	7.11	8.67
MnO	0.14	0.12	0.15	0.10	0.16	0.17	0.16
MgO	3.86	3.85	2.59	3.07	2.43	1.40	2.44
CaO	11.15	10.78	10.75	10.14	11.71	11.96	12.38
Na_2O	3.13	3.13	2.85	2.89	3.04	3.89	2.81
K_2O	2.67	2.74	3.26	2.46	2.67	3.02	2.28
P_2O_5	0.75	0.73	0.68	0.69	0.74	0.76	0.75
S	0.067	0.070	0.095	0.059	0.133	0.133	0.093
Cl	0.158	0.157	0.189	0.173	0.206	0.183	0.179
Total	99.35	98.82	97.75	97.79	98.60	99.34	99.69
Host olivine							
Fo mol %	78.38	78.38	82.39	82.39	82.39	81.25	81.25
SiO_2	38.89	38.89	39.20	39.20	39.20	39.14	39.14
MgO	40.67	40.67	43.40	43.40	43.40	42.81	42.81
FeO	20.00	20.00	16.55	16.55	16.55	17.63	17.63
MnO	0.38	0.38	0.29	0.29	0.29	0.30	0.30
CaO	0.33	0.33	0.28	0.28	0.28	0.27	0.27
Recalculated compositions[b]							
SiO_2	50.88	50.48	50.09	51.64	49.65	50.00	50.00
TiO_2	0.91	0.92	0.87	0.85	0.83	0.98	0.93
Al_2O_3	17.24	17.16	16.83	17.17	17.05	16.95	16.32
FeO_{total}	8.10	8.30	7.88	7.44	8.22	7.48	9.40
MnO	0.14	0.13	0.15	0.11	0.17	0.13	0.17
MgO	4.27	4.38	5.09	4.81	5.31	4.59	5.77
CaO	11.02	10.62	10.08	9.69	10.88	9.67	11.36
Na_2O	3.09	3.08	2.67	2.76	2.82	3.14	2.57
K_2O	2.64	2.70	3.05	2.35	2.47	2.42	2.09
P_2O_5	0.74	0.72	0.64	0.66	0.68	0.57	0.69
S	0.066	0.069	0.095	0.059	0.132	0.055	0.090
Cl	0.156	0.154	0.177	0.165	0.191	0.172	0.164
Total	99.31	98.79	97.71	97.75	98.55	96.20	99.65
S/Cl	0.43	0.45	0.54	0.36	0.69	0.32	0.55
X_{fo}[c]	0.01	0.01	0.07	0.05	0.08	0.04	0.09

[a] S concentration is below detection limits; see text

[b] Melt inclusions recalculated after Luhr, 2001

[C] The fraction of post-entrapment crystallization of olivine

Appendix 8.7. cont.

Pumiceous bombs

	strom1 olv12m1	strom5 olv1m1	strom5 olv2m1	strom5 olv3m1	strom5 olv7m1	strom5 olv8m1	strom5 olv1m1
SiO_2	49.24	53.21	53.77	52.94	50.80	50.82	52.56
TiO_2	0.94	1.74	1.69	1.70	1.92	1.84	1.58
Al_2O_3	18.66	15.92	15.25	15.84	15.97	15.85	16.17
FeO_{total}	8.41	10.10	10.25	10.34	10.39	10.59	9.65
MnO	0.18	0.14	0.12	0.24	0.16	0.20	0.22
MgO	3.64	2.30	2.49	2.03	2.17	1.98	2.53
CaO	11.39	8.31	8.28	8.21	8.66	8.97	7.88
Na_2O	2.80	3.24	2.66	3.63	3.00	3.39	3.12
K_2O	2.50	4.35	4.30	4.23	4.54	4.05	4.61
P_2O_5	0.63	1.13	1.36	1.16	1.28	1.21	1.24
S	0.128	0.025[a]	0.004[a]	0.032[a]	0.025[a]	0.069	0.008[a]
Cl	0.179	0.132	0.138	0.178	0.140	0.155	0.125
Total	98.78	100.60	100.46	100.51	99.04	99.16	99.66
Host olivine							
Fo mol %	82.14	70.81	71.02	70.49	70.47	70.18	70.19
SiO_2	38.08	37.27	37.07	36.699	37.146	37.735	37.018
MgO	43.50	36.03	36.026	35.311	35.295	35.095	35.503
FeO	16.84	26.47	26.221	26.366	26.358	26.536	26.894
MnO	0.29	0.51	0.489	0.495	0.49	0.487	0.474
CaO	0.25	0.36	0.341	0.352	0.358	0.346	0.328
Recalculated compositions[b]							
SiO_2	48.33	52.68	53.39	52.27	50.26	50.18	52.32
TiO_2	0.88	1.69	1.64	1.63	1.85	1.75	1.56
Al_2O_3	17.57	15.40	14.86	15.19	15.37	15.13	15.94
FeO_{total}	8.80	10.62	10.71	11.00	10.97	11.30	9.89
MnO	0.19	0.15	0.13	0.25	0.17	0.22	0.23
MgO	5.68	3.38	3.42	3.40	3.39	3.46	2.99
CaO	10.73	8.05	8.07	7.88	8.34	8.57	7.77
Na_2O	2.63	3.14	2.59	3.48	2.89	3.23	3.07
K_2O	2.35	4.21	4.18	4.06	4.37	3.86	4.54
P_2O_5	0.59	1.10	1.32	1.12	1.23	1.15	1.22
S	0.125	0.024	0.004	0.031	0.024	0.066	0.007
Cl	0.168	0.128	0.134	0.171	0.134	0.147	0.123
Total	98.19	100.57	100.42	100.47	99.01	99.13	99.64
S/Cl	0.74	0.19	0.03	0.18	0.18	0.45	0.06
X_{fo}[c]	0.06	0.03	0.03	0.04	0.04	0.05	0.01

[a] S concentration is below detection limits; see text

[b] Melt inclusions recalculated after Luhr, 2001

[C] The fraction of post-entrapment crystallization of olivine

Appendix 8.7. cont.

Pumiceous bombs

	strom5 olv12m1
SiO_2	54.32
TiO_2	0.98
Al_2O_3	16.64
FeO_{total}	8.83
MnO	0.16
MgO	2.16
CaO	6.28
Na_2O	3.35
K_2O	5.49
P_2O_5	0.72
S	0.042
Cl	0.079
Total	97.66
Host olivine	
Fo mol %	69.99
SiO_2	36.697
MgO	35.079
FeO	26.84
MnO	0.52
CaO	0.323
Recalculated compositions[b]	
SiO_2	53.19
TiO_2	0.95
Al_2O_3	16.09
FeO_{total}	9.04
MnO	0.16
MgO	2.73
CaO	6.08
Na_2O	3.24
K_2O	5.31
P_2O_5	0.69
S	0.040
Cl	0.076
Total	97.64
S/Cl	0.53
X_{fo}[c]	0.02

[a] S concentration is below detection limits; see text

[b] Melt inclusions recalculated after Luhr, 2001

[C] The fraction of post-entrapment crystallization of olivine

Appendix 8.7. cont.

Scoriaceous bombs

	strom07-1 olv2m1	strom07-1 olv2m2	strom07-1 olv3m1	strom07-1 olv17m1	strom07-1 olv17m2	strom07-2 olv2m1	Strom07-2 olv3-m1
SiO_2	51.28	53.32	48.41	51.61	52.88	53.30	53.10
TiO_2	1.29	1.43	1.80	1.49	1.36	1.50	1.51
Al_2O_3	16.57	15.63	15.01	15.36	16.06	15.16	15.25
FeO_{total}	10.13	9.58	11.33	12.10	10.87	9.91	9.95
MnO	0.14	0.20	0.24	0.21	0.20	0.22	0.15
MgO	2.66	2.99	2.78	3.95	3.18	3.41	3.32
CaO	9.68	7.84	11.13	8.25	8.07	7.39	7.39
Na_2O	3.02	3.36	2.35	3.46	2.99	3.45	3.44
K_2O	3.51	4.67	3.63	2.98	3.86	4.31	4.16
P_2O_5	0.80	1.11	2.40	0.79	0.92	0.32	0.40
S	0.038[a]	0.001[a]	0.019[a]	0.075	0.023[a]	0.012[a]	0.004[a]
Cl	0.123	0.125	0.334	0.218	0.111	0.109	0.117
Total	99.26	100.22	99.38	100.50	100.53	99.07	98.78
Host olivine							
Fo mol %	73.83	73.83	72.19	72.61	72.61	73.07	73.11
SiO_2	38.382	38.382	37.745	37.457	37.457	36.72	36.61
MgO	37.082	37.082	36.3	36.826	36.826	37.01	37.21
FeO	23.435	23.435	24.923	24.789	24.789	24.34	24.37
MnO	0.415	0.415	0.461	0.474	0.474	0.49	0.48
CaO	0.368	0.368	0.335	0.34	0.34	0.34	0.32
Recalculated compositions[b]							
SiO_2	50.73	52.98	48.00	51.41	52.52	53.12	52.87
TiO_2	1.24	1.40	1.74	1.47	1.33	1.48	1.49
Al_2O_3	15.90	15.28	14.49	15.18	15.69	15.01	15.04
FeO_{total}	10.65	9.88	11.78	12.23	11.19	10.05	10.14
MnO	0.15	0.20	0.25	0.21	0.21	0.22	0.16
MgO	4.04	3.75	3.92	4.32	3.95	3.74	3.76
CaO	9.30	7.67	10.75	8.16	7.89	7.32	7.29
Na_2O	2.90	3.29	2.27	3.42	2.92	3.41	3.39
K_2O	3.37	4.57	3.50	2.94	3.77	4.27	4.11
P_2O_5	0.77	1.09	2.31	0.78	0.90	0.31	0.40
S	0.036	0.001	0.019	0.070	0.023	0.011	0.004
Cl	0.118	0.122	0.322	0.215	0.108	0.108	0.115
Total	99.23	100.20	99.30	100.45	100.50	99.05	98.75
S/Cl	0.31	0.01	0.06	0.32	0.21	0.11	0.03
X_{fo}[c]	0.04	0.02	0.04	0.01	0.02	0.01	0.01

[a] S concentration is below detection limits; see text

[b] Melt inclusions recalculated after Luhr, 2001

[C] The fraction of post-entrapment crystallization of olivine

Appendix 8.7. cont.

Scoriaceous bombs

	Strom07-2 olv4-m1	Strom07-2 olv4-m2	Strom07-2 olv5-m1	Strom07-2 olv6-m1	Strom07-2 olv6-m2	Strom07-2 olv6-m3	strom07-5 olv1m1
SiO_2	54.55	54.45	54.60	54.69	54.44	54.60	53.70
TiO_2	1.48	1.44	1.47	1.47	1.48	1.45	1.64
Al_2O_3	15.39	14.72	15.39	15.27	14.82	15.31	15.36
FeO_{total}	9.93	9.95	9.91	10.02	9.98	10.07	9.76
MnO	0.27	0.20	0.28	0.20	0.21	0.13	0.16
MgO	3.33	3.22	3.26	3.23	3.31	3.32	2.46
CaO	7.22	7.22	7.74	7.42	7.40	7.45	8.28
Na_2O	3.32	3.48	3.43	3.68	3.52	3.49	3.58
K_2O	4.24	4.23	3.82	4.33	4.07	4.21	4.19
P_2O_5	0.32	0.36	0.31	0.43	0.32	0.36	1.15
S	0.000[a]	0.005[a]	0.002[a]	0.012[a]	0.017[a]	0.000[a]	0.012[a]
Cl	0.122	0.115	0.145	0.120	0.128	0.120	0.136
Total	100.14	99.37	100.31	100.85	99.68	100.47	100.41
Host olivine							
Fo mol %	72.72	72.72	72.60	72.53	72.53	72.53	72.71
SiO_2	36.80	36.80	37.17	37.03	37.03	37.03	37.04
MgO	37.04	37.04	36.99	36.52	36.52	36.52	36.86
FeO	24.77	24.77	24.88	24.65	24.65	24.65	24.64
MnO	0.46	0.46	0.45	0.47	0.47	0.47	0.48
CaO	0.31	0.31	0.32	0.31	0.31	0.31	0.32
Recalculated compositions[b]							
SiO2	54.41	54.24	54.41	54.47	54.27	54.43	53.03
TiO2	1.46	1.42	1.45	1.45	1.46	1.43	1.57
Al2O3	15.27	14.54	15.23	15.08	14.68	15.16	14.74
FeO	10.03	10.12	10.05	10.20	10.11	10.20	10.36
MnO	0.27	0.21	0.28	0.21	0.21	0.13	0.17
MgO	3.58	3.61	3.58	3.64	3.60	3.64	3.83
CaO	7.16	7.14	7.66	7.33	7.33	7.38	7.97
Na2O	3.29	3.44	3.40	3.63	3.49	3.46	3.44
K2O	4.21	4.18	3.78	4.28	4.03	4.17	4.03
P2O5	0.31	0.35	0.30	0.42	0.32	0.35	1.11
S	0.000	0.005	0.002	0.012	0.017	0.000	0.011
Cl	0.121	0.114	0.144	0.119	0.127	0.119	0.131
Total	100.11	99.35	100.27	100.83	99.65	100.44	100.38
S/Cl	0.00	0.05	0.01	0.10	0.13	0.00	0.08
X_{fo}[c]	0.01	0.01	0.01	0.01	0.01	0.01	0.04

[a] S concentration is below detection limits; see text

[b] Melt inclusions recalculated after Luhr, 2001

[C] The fraction of post-entrapment crystallization of olivine

Appendix 8.7. cont.

Scoriaceous bombs

	Strom07-5 olv2m1	strom07-5 olv3m1	strom07-5 olv4m2	strom07-5 olv15m1	strom07-5 olv15
SiO_2	53.91	52.65	52.91	53.86	53.19
TiO_2	1.52	1.56	1.78	1.50	1.58
Al_2O_3	14.99	15.97	15.81	15.55	15.46
FeO_{total}	9.76	9.07	10.17	9.80	10.23
MnO	0.13	0.15	0.25	0.16	0.22
MgO	2.52	1.82	2.41	3.23	3.44
CaO	7.89	8.80	8.63	7.19	7.35
Na_2O	3.41	3.40	3.25	3.32	3.30
K_2O	4.86	4.20	3.94	4.26	4.15
P_2O_5	0.34	1.04	1.11	1.04	1.07
S	0.004[a]	0.008[a]	0.004[a]	0.005[a]	0.002[a]
Cl	0.120	0.123	0.107	0.134	0.128
Total	99.43	98.75	100.35	100.00	100.08
Host olivine					
Fo mol %	73.06	72.66	72.32	71.91	71.91
SiO_2	37.37	37.15	38.48	37.22	37.22
MgO	36.75	37.06	35.92	35.97	35.97
FeO	24.16	24.84	24.46	25.05	25.05
MnO	0.46	0.47	0.45	0.47	0.47
CaO	0.31	0.30	0.32	0.34	0.34
Recalculated compositions[b]					
SiO2	53.27	53.28	52.32	53.80	53.19
TiO2	1.46	1.43	1.70	1.49	1.58
Al2O3	14.42	14.75	15.16	15.51	15.46
FeO	10.31	10.35	10.75	9.84	10.23
MnO	0.14	0.13	0.26	0.16	0.22
MgO	3.83	3.71	3.79	3.30	3.44
CaO	7.60	7.51	8.29	7.17	7.35
Na2O	3.28	3.34	3.11	3.31	3.30
K2O	4.67	4.53	3.78	4.24	4.15
P2O5	0.32	0.66	1.06	1.03	1.07
S	0.004	0.003	0.004	0.005	0.002
Cl	0.115	0.104	0.103	0.134	0.128
Total	99.40	99.78	100.32	99.97	100.08
S/Cl	0.04	0.03	0.00	0.04	0.01
X_{fo}[c]	0.04	0.04	0.04	0.00	0.00

[a] S concentration is below detection limits; see text

Appendix 8.8. Matrix glass from pumiceous and scoriaceous bombs

Pumiceous bombs

	strom1	strom1	strom1	strom1	strom1	strom1
SiO_2	51.91	51.87	51.22	51.60	49.65	50.20
TiO_2	0.92	0.89	0.91	0.91	0.96	0.91
Al_2O_3	17.64	17.55	17.85	17.83	17.47	17.67
FeO_{total}	7.62	8.30	7.86	7.91	7.78	7.86
MnO	0.17	0.17	0.15	0.07	0.13	0.05
MgO	5.60	5.76	5.65	5.57	5.68	5.76
CaO	9.74	9.18	9.60	9.34	9.66	9.73
Na_2O	3.27	2.96	3.14	2.74	2.69	3.20
K_2O	2.83	3.33	2.75	3.43	3.40	2.96
P_2O_5	0.71	0.69	0.65	0.66	0.58	0.68
S	0.035[a]	0.028[a]	0.040	0.023[a]	0.039[a]	0.041
Cl	0.125	0.144	0.129	0.127	0.131	0.125
Total	100.58	100.88	100.09	100.35	98.37	99.28
S/Cl	0.28	0.19	0.31	0.18	0.30	0.33

	strom1	strom1	strom1	strom1	strom1	strom1
SiO_2	50.11	51.61	52.04	50.53	51.25	51.36
TiO_2	0.89	0.87	0.89	0.97	0.92	0.95
Al_2O_3	17.99	18.04	17.70	17.85	17.74	17.72
FeO_{total}	8.00	7.16	7.95	8.29	7.94	8.01
MnO	0.13	0.10	0.25	0.17	0.24	0.25
MgO	5.91	5.89	5.79	5.18	5.34	5.55
CaO	9.89	10.96	9.80	10.23	9.97	9.98
Na_2O	2.79	3.01	2.96	2.37	3.10	3.00
K_2O	3.49	1.96	2.67	3.66	2.64	2.77
P_2O_5	0.63	0.69	0.68	0.62	0.60	0.62
S	0.045	0.039[a]	0.026[a]	0.052	0.062	0.049
Cl	0.124	0.102	0.115	0.147	0.143	0.130
Total	100.09	100.46	100.87	100.08	99.97	100.41
S/Cl	0.36	0.38	0.23	0.35	0.43	0.37

[a] S concentration is below detection limits; see text

Appendix 8.8.cont.

Pumiceous bombs

	strom1	strom1	strom1	strom1	strom1	strom1
SiO_2	51.39	50.18	50.44	51.17	51.90	51.60
TiO_2	0.87	0.91	0.85	0.87	0.90	0.85
Al_2O_3	17.48	17.65	17.61	17.59	17.50	17.60
FeO_{total}	7.44	8.27	7.55	7.80	7.36	7.78
MnO	0.11	0.04	0.10	0.21	0.23	0.15
MgO	5.49	5.77	5.44	5.48	5.53	5.60
CaO	9.93	10.39	9.82	9.90	9.98	9.92
Na_2O	2.97	2.97	3.07	3.01	3.03	2.88
K_2O	2.89	2.40	3.24	3.04	2.84	2.87
P_2O_5	0.67	0.71	0.72	0.73	0.74	0.73
S	0.043	0.043	0.029[a]	0.024[a]	0.028[a]	0.018[a]
Cl	0.119	0.136	0.132	0.131	0.137	0.125
Total	99.42	99.46	99.00	99.94	100.17	100.11
S/Cl	0.36	0.31	0.22	0.18	0.20	0.14

	strom1	strom1	strom1	strom1	strom1	strom1
SiO_2	50.20	50.28	51.30	51.01	51.33	50.82
TiO_2	0.90	0.88	0.89	0.91	0.90	0.93
Al_2O_3	17.75	17.72	17.33	17.68	17.70	17.90
FeO_{total}	7.60	7.72	7.83	7.89	7.46	8.06
MnO	0.20	0.12	0.16	0.12	0.16	0.16
MgO	5.51	5.54	5.53	5.42	5.14	5.38
CaO	9.86	9.96	10.04	9.93	9.88	10.09
Na_2O	2.93	2.81	3.01	2.88	3.09	2.96
K_2O	2.84	2.73	2.78	2.39	2.98	2.38
P_2O_5	0.60	0.68	0.74	0.64	0.60	0.69
S	0.041	0.057	0.026[a]	0.011[a]	0.019[a]	0.025[a]
Cl	0.117	0.116	0.127	0.140	0.162	0.126
Total	98.55	98.65	99.74	99.00	99.39	99.52
S/Cl	0.35	0.49	0.20	0.08	0.11	0.20

[a] S concentration is below detection limits; see text

Appendix 8.8.cont.

Pumiceous bombs

	strom1	strom1	strom1	strom1	strom1	strom1
SiO_2	50.72	50.22	51.71	50.55	51.40	51.13
TiO_2	0.88	0.89	0.85	0.85	0.86	0.98
Al_2O_3	18.16	18.19	18.04	18.16	18.15	18.10
FeO_{total}	7.66	8.18	8.12	7.88	7.62	7.65
MnO	0.19	0.17	0.19	0.13	0.19	0.10
MgO	5.20	5.42	5.20	5.25	5.28	5.23
CaO	9.89	9.90	9.94	9.88	10.06	10.06
Na_2O	3.25	2.13	2.10	2.24	1.87	1.86
K_2O	2.92	2.79	2.91	3.09	2.88	2.82
P_2O_5	0.62	0.73	0.74	0.57	0.56	0.76
S	0.027[a]	0.057	0.027[a]	0.029[a]	0.038[a]	0.033[a]
Cl	0.197	0.126	0.126	0.151	0.137	0.140
Total	99.69	98.82	99.94	98.79	99.06	98.86
S/Cl	0.14	0.45	0.21	0.19	0.28	0.23

	strom1	strom1	strom1	strom1	strom1	strom1
SiO_2	50.32	51.18	50.60	50.96	51.50	50.18
TiO_2	0.90	0.89	0.93	0.89	0.87	0.87
Al_2O_3	18.04	18.31	18.00	18.07	18.11	17.72
FeO_{total}	7.60	7.83	7.79	7.60	7.77	7.88
MnO	0.17	0.20	0.13	0.24	0.22	0.13
MgO	5.32	5.27	5.41	5.21	5.32	5.43
CaO	9.93	9.88	9.93	10.06	10.00	10.12
Na_2O	2.11	2.17	1.96	2.14	2.05	2.32
K_2O	2.72	2.82	2.75	2.82	2.79	2.81
P_2O_5	0.67	0.70	0.68	0.65	0.67	0.70
S	0.041	0.032[a]	0.041	0.006[a]	0.033[a]	0.041
Cl	0.136	0.132	0.153	0.146	0.137	0.143
Total	97.97	99.39	98.37	98.75	99.48	98.35
S/Cl	0.30	0.24	0.27	0.04	0.24	0.28

[a] S concentration is below detection limits; see text

Appendix 8.8.cont.

Pumiceous bombs

	strom1	strom1	strom1	strom1	strom1	strom1
SiO_2	50.18	51.34	51.62	50.93	49.89	50.89
TiO_2	0.92	0.87	0.90	0.85	0.88	0.87
Al_2O_3	17.85	17.87	17.94	17.94	17.94	18.15
FeO_{total}	7.62	7.82	7.77	8.20	7.34	7.60
MnO	0.13	0.09	0.13	0.22	0.11	0.13
MgO	5.32	5.25	5.28	5.36	5.51	5.28
CaO	10.03	9.87	9.94	9.98	9.99	9.90
Na_2O	1.82	2.17	2.18	2.58	2.55	2.60
K_2O	2.96	2.97	2.89	2.85	2.74	2.90
P_2O_5	0.68	0.68	0.64	0.70	0.72	0.73
S	0.043	0.029[a]	0.028[a]	0.008[a]	0.023[a]	0.024[a]
Cl	0.163	0.155	0.155	0.138	0.145	0.126
Total	97.73	99.09	99.45	99.71	97.83	99.18
S/Cl	0.26	0.19	0.18	0.05	0.16	0.19

	strom1	strom1	strom5b	strom5b	strom5b	strom5b
SiO_2	49.93	51.26	51.00	51.23	50.10	49.62
TiO_2	0.86	0.90	0.92	0.90	0.98	0.91
Al_2O_3	18.07	18.03	17.54	17.50	17.23	17.87
FeO_{total}	7.84	7.55	8.09	7.51	8.43	8.31
MnO	0.13	0.13	0.23	0.14	0.24	0.20
MgO	5.32	5.20	5.81	5.61	5.46	6.13
CaO	9.97	9.97	11.75	11.68	11.81	11.46
Na_2O	2.74	2.61	2.58	2.40	2.42	2.41
K_2O	2.81	2.78	1.94	1.98	2.32	2.13
P_2O_5	0.64	0.69	0.69	0.77	0.71	0.65
S	0.017[a]	0.020[a]	0.008[a]	0.019[a]	0.014[a]	0.016[a]
Cl	0.132	0.124	0.130	0.099	0.081	0.129
Total	98.43	99.26	100.66	99.85	99.87	99.82
S/Cl	0.13	0.16	0.06	0.19	0.17	0.12

[a] S concentration is below detection limits; see text

Appendix 8.8.cont.

Pumiceous bombs

	strom5b	strom5b	strom5b	strom5b	strom5b	strom5b
SiO_2	49.12	49.08	49.01	48.90	53.49	50.25
TiO_2	0.87	0.87	0.95	0.92	1.57	1.00
Al_2O_3	17.87	17.90	17.77	17.87	15.60	18.07
FeO_{total}	7.65	8.02	8.10	8.43	9.97	8.40
MnO	0.16	0.13	0.20	0.10	0.23	0.16
MgO	6.14	6.50	6.45	6.38	3.40	5.82
CaO	11.15	11.39	11.62	11.73	7.87	11.57
Na_2O	2.78	2.43	2.53	2.58	3.23	2.43
K_2O	2.08	2.06	2.05	2.10	4.04	2.01
P_2O_5	0.71	0.63	0.76	0.73	1.02	0.66
S	0.019[a]	0.015[a]	0.022[a]	0.017[a]	0.000[a]	0.027[a]
Cl	0.123	0.098	0.103	0.120	0.114	0.109
Total	98.66	99.11	99.55	99.86	100.51	100.50
S/Cl	0.15	0.15	0.21	0.14	0.00	0.24

	strom5b
SiO_2	49.72
TiO_2	0.95
Al_2O_3	18.27
FeO_{total}	8.28
MnO	0.17
MgO	5.86
CaO	11.85
Na_2O	2.47
K_2O	1.95
P_2O_5	0.68
S	0.012[a]
Cl	0.102
Total	100.29
S/Cl	0.11

[a] S concentration is below detection limits; see text

Appendix 8.8.cont.

Scoriaceous bombs

	strom07-1	strom07-1	strom07-1	strom07-1	strom07-1	strom07-1
SiO_2	53.77	53.68	53.12	53.44	54.06	54.51
TiO_2	1.39	1.45	1.44	1.38	1.42	1.49
Al_2O_3	15.69	15.53	15.60	15.33	15.31	15.39
FeO_{total}	9.22	10.29	9.96	9.53	8.87	8.53
MnO	0.21	0.27	0.22	0.23	0.26	0.21
MgO	3.29	3.48	3.34	3.49	3.15	3.11
CaO	7.66	6.23	6.64	7.76	6.90	7.10
Na_2O	3.62	3.54	3.55	3.61	3.77	3.89
K_2O	4.20	4.91	4.66	4.14	4.79	4.57
P_2O_5	1.03	1.04	0.94	1.04	0.29	0.33
S	0.000[a]	0.008[a]	0.001[a]	0.007[a]	0.000[a]	0.001[a]
Cl	0.106	0.131	0.133	0.103	0.128	0.126
Total	100.15	100.53	99.57	100.04	98.91	99.22
S/Cl	0.00	0.06	0.00	0.07	0.00	0.01

	strom07-1	strom07-1	strom07-1	strom07-1	strom07-1	strom07-2
SiO_2	53.76	54.45	54.52	54.21	53.73	53.72
TiO_2	1.44	1.49	1.45	1.50	1.48	1.45
Al_2O_3	15.32	15.72	15.20	15.46	15.45	15.13
FeO_{total}	8.97	10.10	9.68	9.49	10.13	9.31
MnO	0.15	0.19	0.22	0.21	0.19	0.12
MgO	2.69	3.15	3.26	3.15	3.40	3.41
CaO	8.92	6.88	7.06	7.46	7.49	7.18
Na_2O	3.37	3.38	3.39	3.47	3.50	3.87
K_2O	4.30	4.49	4.66	4.59	3.78	4.48
P_2O_5	0.37	0.34	0.30	0.33	1.07	1.00
S	0.011[a]	0.005[a]	0.006[a]	0.000[a]	0.009[a]	0.009[a]
Cl	0.116	0.107	0.118	0.119	0.124	0.117
Total	99.40	100.29	99.84	99.95	100.32	99.76
S/Cl	0.10	0.04	0.05	0.00	0.07	0.08

[a] S concentration is below detection limits; see text

Appendix 8.8.cont.

Scoriaceous bombs

	strom07-2	strom07-2	strom07-2	strom07-2	strom07-2	strom07-2
SiO_2	52.88	53.91	53.29	52.12	51.77	53.66
TiO_2	1.42	1.45	1.41	1.45	1.40	1.45
Al_2O_3	15.38	15.63	15.09	14.97	15.74	15.16
FeO_{total}	9.97	9.80	10.40	10.77	9.18	9.97
MnO	0.16	0.12	0.13	0.27	0.13	0.18
MgO	3.51	3.49	3.59	3.68	3.29	3.44
CaO	7.51	7.58	7.41	7.74	7.42	7.42
Na_2O	3.31	3.34	3.41	3.50	3.63	3.38
K_2O	4.23	4.26	4.38	3.93	5.00	4.16
P_2O_5	1.05	0.97	1.00	1.08	1.04	0.94
S	0.004[a]	0.006[a]	0.002[a]	0.005[a]	0.005[a]	0.012[a]
Cl	0.114	0.095	0.093	0.111	0.116	0.113
Total	99.50	100.63	100.16	99.60	98.70	99.86
S/Cl	0.04	0.06	0.02	0.05	0.04	0.11

	strom07-2	strom07-2	strom07-2	strom07-2	strom07-2	strom07-2
SiO_2	52.99	53.00	54.03	54.79	53.44	54.09
TiO_2	1.48	1.44	1.47	1.46	1.41	1.43
Al_2O_3	15.43	15.34	15.41	15.58	15.31	15.46
FeO_{total}	9.71	9.28	9.84	9.75	9.60	9.31
MnO	0.13	0.20	0.25	0.27	0.15	0.18
MgO	3.45	3.37	3.33	3.29	3.33	3.26
CaO	7.35	7.37	7.46	7.41	7.40	7.32
Na_2O	3.58	3.27	3.44	3.59	3.17	3.73
K_2O	4.43	5.12	4.22	4.19	4.65	4.28
P_2O_5	1.05	1.00	0.31	0.30	0.33	0.32
S	0.009[a]	0.003[a]	0.008[a]	0.008[a]	0.000[a]	0.008[a]
Cl	0.110	0.113	0.110	0.106	0.098	0.104
Total	99.68	99.46	99.85	100.74	98.88	99.49
S/Cl	0.08	0.02	0.08	0.07	0.00	0.08

[a] S concentration is below detection limits; see text

Appendix 8.8.cont.

Scoriaceous bombs

	strom07-2	strom07-2	strom07-2	strom07-2	strom07-2	strom07-2
SiO_2	54.03	53.02	54.27	54.44	54.68	54.53
TiO_2	1.42	1.40	1.51	1.44	1.50	1.45
Al_2O_3	15.31	15.41	15.30	15.33	15.50	15.59
FeO_{total}	9.58	9.80	9.38	9.73	9.24	9.38
MnO	0.15	0.06	0.27	0.31	0.20	0.28
MgO	3.29	3.23	3.32	3.38	3.26	3.39
CaO	7.35	7.38	7.24	7.47	7.23	7.48
Na_2O	3.41	3.17	3.84	3.46	3.68	3.67
K_2O	4.77	5.37	4.38	4.18	4.29	4.32
P_2O_5	0.41	0.35	0.31	0.34	0.37	0.36
S	0.010[a]	0.000[a]	0.010[a]	0.007[a]	0.000[a]	0.008[a]
Cl	0.098	0.118	0.112	0.112	0.095	0.116
Total	99.81	99.31	99.93	100.16	100.03	100.56
S/Cl	0.10	0.00	0.09	0.06	0.00	0.07

	strom07-5	strom07-5	strom07-5	strom07-5	strom07-5	strom07-5
SiO_2	54.07	53.23	53.31	53.93	54.32	53.80
TiO_2	1.42	1.45	1.50	1.46	1.47	1.53
Al_2O_3	15.76	15.37	15.66	15.69	15.54	15.53
FeO_{total}	9.04	9.27	9.51	10.05	9.69	9.57
MnO	0.19	0.19	0.12	0.17	0.17	0.15
MgO	3.17	3.06	3.39	3.30	3.36	3.41
CaO	7.77	7.79	7.37	7.28	7.49	7.31
Na_2O	4.29	4.21	3.30	3.44	3.12	3.38
K_2O	2.58	2.52	4.45	4.30	4.54	4.41
P_2O_5	0.92	1.10	1.05	1.01	1.00	0.99
S	0.005[a]	0.006[a]	0.015[a]	0.005[a]	0.000[a]	0.012[a]
Cl	0.109	0.096	0.119	0.113	0.127	0.117
Total	99.30	98.28	99.77	100.73	100.80	100.19

a.

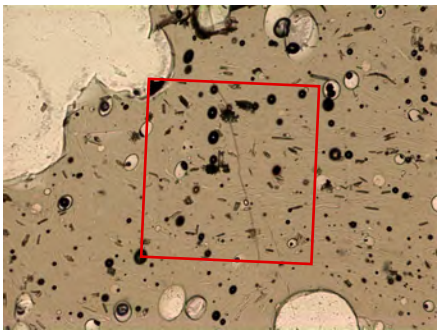

b.

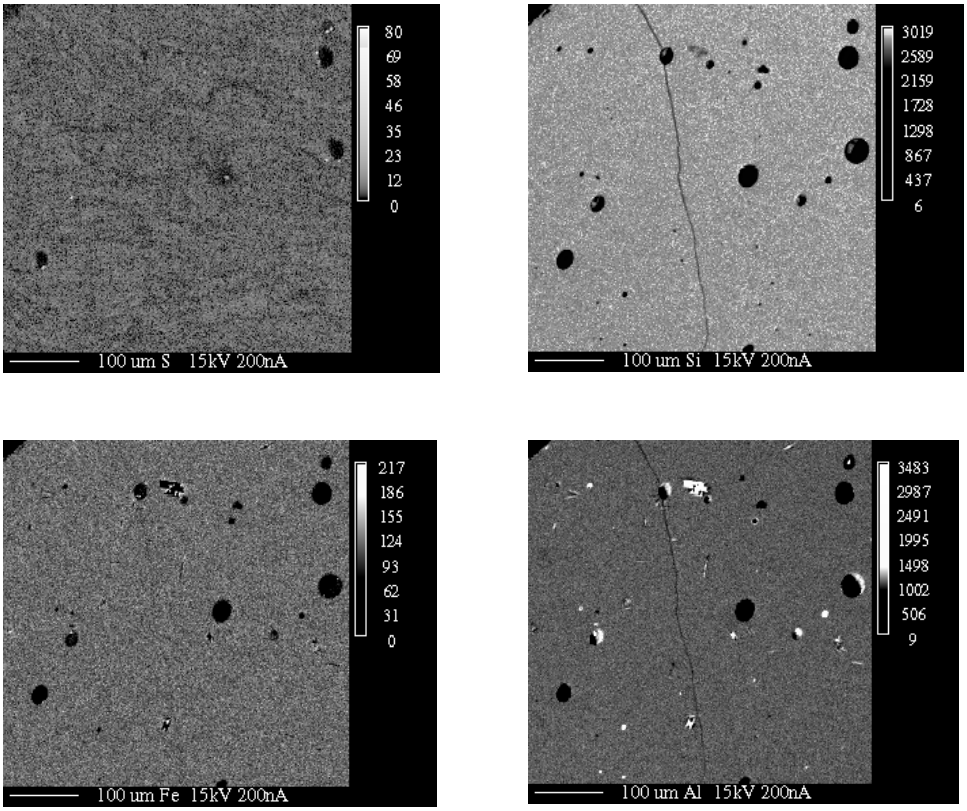

Appendix 8.9. Dot maps of glass next to vesicles. a. Photomicrograph of analyzed area. b. Slight variations in S can be seen in the form of banding. This banding is not seen other major elements Si, Fe, or Al, however.